Preclinical anti-cancer activity and multiple mechanisms of action of a cationic silver complex bearing N-heterocyclic carbene ligands.

ALLISON, Simon J., SADIQ, Maria, BARONOU, Efstathia, COOPER, Patricia A., DUNNILL, Chris, GEORGOPOULOS, Nik <http://orcid.org/0000-0002-6330-4947>, LATIF, Ayşe, SHEPHERD, Samantha, SHNYDER, Steve D., STRATFORD, Ian J., WHEELHOUSE, Richard T., WILLANS, Charlotte E. and PHILLIPS, Roger M.

Preclinical anti-cancer activity and multiple mechanisms of action of a cationic silver complex bearing N-heterocyclic carbene ligands.

Simon J Allison[a], Maria Sadiq[b], Efstathia Baronou[c], Patricia A Cooper[b], Chris Dunnill[a], Nikolaos T Georgopoulos[a], Ayşe Latif[d], Samantha Shepherd[a], Steve D Shnyder[b], Ian J Stratford[d], Richard Wheelhouse[c], Charlotte Willans[e] and Roger M Phillips[a]

[a] School of Applied Sciences, University of Huddersfield, Queensgate, Huddersfield HD1 3DH, UK.

[b] Institute of Cancer Therapeutics, University of Bradford, Bradford BD7 1DP, UK.

[c] School of Pharmacy, University of Bradford, Bradford BD7 1DP, UK.

[d] Division of Pharmacy and Optometry, Stopford Building, University of Manchester, Oxford Road, Manchester M13 9PT

[e] School of Chemistry, University of Leeds, Woodhouse Lane, Leeds, LS2 9JT UK.

Author for correspondence: Roger M Phillips, Department of Pharmacy, School of Applied Sciences, University of Huddersfield, Queensgate, Huddersfield HD1 3DH, UK. Tel: 01484 471675, E-mail: r.m.phillips@hud.ac.uk

Abstract

Organometallic complexes offer the prospect of targeting multiple pathways that are important in cancer biology. Here, the preclinical activity and mechanism(s) of action of a silver-bis(N-heterocyclic carbine) complex (Ag8) were evaluated. Ag8 induced DNA damage via several mechanisms including topoisomerase I/II and thioredoxin reductase inhibition and induction of reactive oxygen species. DNA damage induction was consistent with cytotoxicity observed against proliferating cells and Ag8 induced cell death by apoptosis. Ag8 also inhibited DNA repair enzyme PARP1, showed preferential activity against cisplatin resistant A2780 cells and potentiated the activity of temozolomide. Ag8 was substantially less active against non-proliferating non-cancer cells and selectively inhibited glycolysis in cancer cells. Ag8 also induced significant anti-tumour effects against cells implanted intraperitoneally in hollow fibres but lacked activity against hollow fibres implanted subcutaneously. Thus, Ag8 targets multiple pathways of importance in cancer biology, is less active against non-cancer cells and shows activity *in vivo* in a loco-regional setting.

Key words:

- Silver-N-heterocyclic carbene
- Thioredoxin reductase inhibitor
- Topoisomerase inhibitor
- PARP1 inhibitor
- Glycolytic inhibitor

1. Introduction

An increased understanding of the molecular and cellular biology of cancer has led to an explosion of research into targeted therapies. For certain cancers harbouring particular genetic lesions, targeted therapies have led to significant improvements in outcomes but their use is not without significant limitations. Resistance to treatment remains a significant problem [1] and novel strategies are required to tackle the challenges of tumour plasticity and heterogeneity that promote the development of resistance [2]. One such strategy that is particularly applicable to complex diseases such as cancer is the development of a single drug that targets multiple pathways, an approach known as polypharmacology [3, 4]. This approach has the potential to target biologically important networks thereby reducing the impact of plasticity and heterogeneity but it carries the inherent risk of widespread toxicity. The challenge is to identify multi-targeted agents that exhibit selectivity for cancer cells over normal cells [5].

Within this context, there is resurging interest in organometallic complexes following the demonstration that they can target multiple biochemical pathways with cytotoxic activity that is independent of binding to nucleic acids [6]. Metal complexes with *N*-heterocyclic carbene (NHC) ligands have emerged as an interesting class of organometallic compounds that have anti-microbial and anti-cancer activity [7]. Gold-NHC complexes have been the focus of research into new anti-cancer drugs but these have shown undesirable toxicity *in vivo* including oxidative damage to the heart and reproductive toxicity in rats [8]. In contrast to gold-NHC complexes, silver-NHC complexes have the potential advantage of reduced toxicity as silver inherently lacks toxicity. This together with the increased stability of silver-NHC complexes make this class of compound particularly attractive as potential anti-cancer drugs [9]. We recently reported the synthesis and initial evaluation of a series of novel silver-NHC complexes that demonstrated cytotoxic activity against MCF7 (human breast carcinoma) and DLD-1 (human colo-rectal carcinoma) cell lines *in vitro* [10]. Of these compounds, $Ag(NHC)_2AgBr_2$ (Ag8, Figure 1) was identified as suitable for further evaluation. The purpose of this study was to determine the mechanism(s) of action of Ag8 in the context of identifying a multi-targeted agent that retained selectivity for cancer as opposed to non-cancer cells.

2. Material and Methods

2.1 Compounds: Ag8 was synthesised as described previously [10]. Cisplatin, etoposide, temozolomide (TMZ) and NU1025 were obtained from Sigma Aldrich (Poole, Dorset, UK).

2.2 Cell Lines: A panel of 16 human cancer and 3 human non-cancer cells was selected for this study, details of which are presented in Table S1. Cells were cultured in complete medium with appropriate supplements as recommended by ATCC or ECACC.

2.3 Chemosensitivity studies: Cell lines were seeded in 96-well plates at 2000 cells/well and allowed to adhere overnight. Cells were exposed to a range of drug concentrations for 96 h after which cell survival was determined using the MTT assay [11]. The selectivity index (SI) was defined as the IC_{50} for non-cancer cells divided by the IC_{50} for cancer cells (values >1 indicating selectivity for cancer cells). Ag8 was also submitted to the National Cancer Institute (Bethesda, USA) for evaluation in the NCI60 cell line panel (NSC 767019).

2.4 Inhibition of Thioredoxin Reductase 1 (Trx-R): The effect of Ag8 on Trx-R activity was determined using the substrate 5,5'-dithiobis-(2-nitrobenzoic acid) (DTNB) as described elsewhere [12, 13]. Inhibition of Trx-R activity in Ag8 treated samples was calculated as a percentage of enzyme activity of vehicle treated controls.

2.5 Detection of Reactive Oxygen Species (ROS): Cells were seeded at a density of $3x10^6$ in $10cm^2$ tissue culture dishes and allowed to adhere overnight. Cells were then treated for 30 minutes with cisplatin (10μM), Ag8 (10μM) or appropriate vehicle controls, washed twice with PBS, and labelled with H2-DCFDA (4μM) (Life Technologies) at 37 °C in PBS for 30 minutes. Cells were then washed with ice-cold with PBS before trypsinisation and resuspension in ice-cold PBS for immediate analysis for ROS levels by flow cytometry.

2.6 Effect of the anti-oxidant N-acetyl-cysteine (NAC) on the cytotoxic activity of Ag8: Ovarian cancer cells were pre-treated for 1 h with NAC (1 mM) followed by cisplatin or Ag8 in 1mM NAC for a further 72 h. Total cell biomass was assessed using the colorimetric CellTiter 96® AQueous One Solution Cell proliferation assay (Promega).

2.7 Detection of stress-activated protein kinases: Cells were treated for 0, 1.5, 3 and 6 hours with either cisplatin (10μM) or Ag8 (10μM), lysed and processed for SDS-PAGE and immunoblotting using antibodies for p-JNK, pSAPK/JNK, p-38, p-38 MAPK and β-actin as previously described [14].

2.8 Induction of apoptosis: Apoptosis was detected using the Annexin-V-FLUOS Staining Kit (Roche) as previously described [15]. Briefly, A2780 and A2780*cis*/CP70 cells were seeded at $1x10^5$ cells/well in 6 well plates, incubated overnight at 37 °C and exposed to Ag8 (10μM), cisplatin (10μM) or etoposide (10μM) for 24 h at 37 °C. Cells were labelled with Annexin and propidium iodide as described by the manufacturer and analysed by flow cytometry.

2.9 DNA UV Thermal Melting Studies: These were performed as previously described [16]. Calf thymus DNA (ctDNA) (Sigma Aldrich, Poole, UK) was exposed to Ag8 and DNA thermal melting curves were determined using a Varian-Cary 400 Bio UV/Vis spectrophotometer, equipped with a Peltier temperature controller. Heating runs were performed between 25 and 99 °C, heating at a rate of 1 °C min^{-1}, while continuously monitoring the absorbance at 260 nm. Melting temperatures (T_m) were determined graphically from the primary data using the method of Wilson et al [17].

2.10 Induction of DNA damage in cell free assays: The ability of Ag8 to directly damage supercoiled plasmid DNA was assessed as described in detail previously [18]. Briefly, supercoiled plasmid DNA was exposed to a range of Ag8 concentrations for 1 h at 37 °C, separated on a 1% agarose gel prior to staining with ethidium bromide. Images were captured on a FX phosphoimager using Image Q software (Biorad).

2.11 Induction of DNA damage in cells: The induction of DNA damage in A2780 and A2780*cis*/CP70 cells was performed using the alkaline and neutral comet assay as previously described [19, 20]. Comets were visualised using an epifluorescent microscope (Nikon Eclipse E800, Japan) with images captured and tail moments determined for 50 randomly selected comets using Comet assay III software (Perceptive Instruments, UK).

2.12 Inhibition of topoisomerase I and II: The effect of Ag8 on topoisomerase activity was determined using human topoisomerase I and II relaxation assays (Inspiralis, Norwich, UK). Reaction conditions were as specified by the manufacturer with the topoisomerase reaction mix incubated with Ag8 (various concentrations) for 5 min prior to the addition of supercoiled plasmid DNA. The bioreductive prodrug EO9 was used as a positive control for the induction of single strand breaks in DNA [11]. Following a 30 min incubation at 37 °C, supercoiled and relaxed plasmid DNA was separated on a 1% agarose gel, stained with ethidium bromide and visualised using Molecular Imager FX (Biorad, Hemel Hempsted, UK).

2.13 Inhibition of PARP-1: The effect of Ag8 and NU1025 on purified PARP-1 activity was determined using the PARP-1 activity assay from Trevigen (Gaithersburg, USA). To assay whether Ag8 inhibits PARP activity in cultured cells, HCT116 colorectal cancer cells were treated with TMZ (1mM) for 2 h to induce SSBs. Cells were washed twice with PBS before a further 15h 'repair' incubation in fresh cell culture medium in the presence or absence of Ag8 (16μM) or NU1025 (100μM). Cells were then stained for S139P γH2AX expression according to the manufacturer's instructions (Cell Signalling Technology) and images were acquired using a Leica fluorescent microscope. As inhibition of PARP has been shown to potentiate TMZ activity [21], HCT116 cells were treated with TMZ (500μM) in the presence or absence of Ag8 or NU1025 and cell survival determined as described above.

2.14 Effects on glycolysis: Glycolysis stress tests (extracellular flux analysis [XF]) were performed using an XF^e96 Analyzer (Seahorse Bioscience) according to the manufacturer's instructions. Briefly, A2780 and OVCAR cells were seeded at $1.5x10^4$ and non-cancer ARPE-19 cells were seeded at $3x10^4$ cells per well. A range of Ag8 concentrations were added to cells just prior to (acute) or 0.5 h and 1 h before assaying glycolytic activity. Three sequential measurements were used to calculate glycolytic parameters for each test condition. To normalize data, cells were stained with sulforhodamine B (SRB) to determine cellular protein content.

2.15 *In vivo* activity of Ag8 in the hollow fibre (HF) assay: All animal procedures were carried out under a project licence issued by the UK Home Office and UK National Cancer Research Institute Guidelines for the Welfare of Animals [22] were followed throughout.

A2780, A2780*cis*/CP70 or OVCAR-3 cells were loaded into sterilised colour-coded PVDF Spectra/Por hollow fibres (Spectrum Medical Inc, Houston, TX, USA) as described previously [23]. Hollow fibres were implanted intraperitoneally (ip) or subcutaneously (sc) and groups of 5 mice were treated with 10 $mgkg^{-1}$ Ag8 in 10% DMSO: 90% arachis oil administered ip daily on days 3, 4, 5 and 6 post-implantation. Cell survival was assessed as described previously [23].

3.0 Results

3.1 Chemosensitivity studies: As expected, the cisplatin resistant A2780*cis*/CP70 cell line was significantly ($p < 0.01$) less responsive to cisplatin than A2780 cells with IC_{50} values of 6.07 ± 1.78 and 0.73 ± 0.30 μM respectively (Figure 2A). In contrast, Ag8 was significantly ($p < 0.001$) more active against the cisplatin resistant A2780cis/CP70 cell line compared to cisplatin sensitive A2780 cells (IC_{50} values of 0.09 ± 0.01 and 0.44 ± 0.15 μM respectively). Against other cancer cells, a broad range of responses to cisplatin was observed with IC_{50} values ranging from 0.56 ± 0.32 μM (MDA-MB-468) to 9.33 ± 2.26 μM (MDA-MB-231). Ag8 showed promising low micromolar activity against all cancer cell lines tested but, with the exception of A2780 and A2780cis/CP70 cells, the range of responses was narrower (6.27 ± 0.39 to 13.34 ± 2.16 μM) than for cisplatin.

The activity of Ag8 and cisplatin against ARPE-19, WI38 and PNT2 non-cancer cells is presented in Table S2 and these IC_{50} values were used to determine the selectivity index presented in Figure 2B. Ag8 exhibited superior selectivity *in vitro* towards the A2780 and A2780cis/CP70 cells over cisplatin for all three non-cancer cells tested (Figure 2B). Similar results were obtained in other cell lines where Ag8 exhibited superior or comparative selectivity to cisplatin (Figure S1). Against the NCI60 tumour cell line panel (Figure S2) no obvious disease specific activity was observed and COMPARE analysis demonstrated that Ag8 does not share a mechanism of action with established anti-cancer drugs including cisplatin. Using the All Synthetic Compounds database however, a correlation coefficient of 0.785 was obtained with Pleurotin, a known inhibitor of Trx-R.

3.2 Induction of Oxidative Stress: In a cell free assay, Ag8 is a potent inhibitor of purified human Trx-R with an IC_{50} of 2.39 ± 0.59nM (Figure 3A). In cells, Trx-R decreases levels of ROS, reducing cellular oxidative stress. The effects of Ag8 on cellular ROS were therefore analysed. Treatment with Ag8 (10 μM , 30 min) caused a ~35% increase in ROS compared

with a 6% increase with cisplatin (10μM) (Figure 3B). Moreover, the anti-oxidant N-acetyl cysteine (NAC) significantly attenuated Ag8 cytotoxicity suggesting that its activity may be partially attributed to Trx-R inhibition and increased ROS production (Figure 3C). Ag8 also caused significant and sustained induction of both p-p38 and p-JNK in both A2780 and A2780cis/CP70 cells (Figure 3D) whereas the effects of cisplatin on p-p38 and p-JNK were transient or markedly smaller, consistent with the observed weaker ROS induction. Significantly, prolonged p-p38 and JNK activation can induce downstream signalling pathways leading to cellular apoptosis and as shown in Figure 4, Ag8 induced significant levels of apoptosis (but not autophagy, Figure S3) in both A2780 and A2780*cis*/CP70 cells. Ag8 had no effect on HIF1α expression or activity (Figure S4).

3.3 Interaction of Ag8 with DNA: UV thermal melting profiles for ctDNA in the absence and presence of Ag8 revealed a concentration dependent shift of T_m indicating that Ag8 stabilises genomic DNA (Figure 5A). The melting profile at higher temperatures shifted disproportionately to the right indicating a preference for stabilisation of GC- over AT-rich sequences (Figures 5A and S5). Whilst Ag8 can bind to DNA, it did not directly cause DNA damage in the form of single (SSB) or double strand breaks (DSB) in supercoiled plasmid DNA in cell-free assays (Figure 5B). In contrast, extensive SSB and DSB DNA damage was observed in A2780 and A2780*cis*/CP70 cells exposed to Ag8 as determined by the alkaline and neutral comet assays (Figures 5C and D). In contrast to cisplatin, no DNA cross linking was detected in either cell line (Figures 5E and S6). In addition to increased ROS (Figure 3B) which can result in DNA damage, Ag8 also proved to be a potent inhibitor of topoisomerases in cell-free assays (Figure 5F). Ag8 caused a significant dose-dependent inhibition of both human topoisomerase I and II with preferential inhibition of topoisomerase I (complete inhibition at 0.16 μM) over topoisomerase II (Figure 5F).

3.4 Inhibition of PARP-1 by Ag8: Ag8 is a very potent inhibitor of purified human PARP-1 with a nanomolar IC_{50} (32 ± 7.6 nM, Figure 6A). Under identical experimental conditions, NU1025 was ~75-fold less potent (IC_{50} of 2.4 ± 0.27 μM). To determine the effect of Ag8 on PARP-mediated DNA repair in cultured cells, the effects of Ag8 on SSB repair, which is PARP-dependent, were determined following treatment with TMZ (Figure 6B). As expected, HCT116 cells treated with TMZ alone showed little or no phosphorylated γH2AX (Figure 6C, *negative control*). In contrast, for 'repairing' cells incubated in the presence of NU1025,

a clear increase in S139P γH2AX positive cells was visible, consistent with inhibition of PARP (Figure 6D). Ag8 treatment alone induced some increase in phosphorylated γH2AX levels (Figure 6E) which is consistent with induction of DSBs as was detected by the neutral comet assay (Figure 5D). However, levels of phosphorylated γH2AX (S139P) were substantially enhanced in cells treated with TMZ plus Ag8 (Figure 6F). Consistent with this, both NU1025 and Ag8 increased the activity of TMZ in drug combination studies (Figure 6G).

3.5 Inhibition of glycolysis by Ag8: Ag8 significantly reduced glycolysis and glycolytic reserve in a dose and time dependent manner in A2780 and OVCAR3 cells (Figures 7A and B). In contrast, 1μM Ag8 had no inhibitory effect on glycolysis and glycolytic reserve in confluent, non-replicating ARPE-19 cells (Figures 7A and B). A small increase in EACR was however observed in ARPE-19 cells (Figure 7A) but this effect was transient and did not reach statistical significance. The effects of Ag8 glycolysis and glycolytic reserve were concentration and exposure time with no acute effects on cell number observed (Figure S7 and S8).

3.6 Anti-tumour activity of Ag8 against ovarian cancers in hollow fibres *in vivo*: A single dose of up to 20 $mgkg^{-1}$ given i.p. or 10 $mgkg^{-1}$ administered i.p. (daily for 4 days) was well tolerated with no loss in body weight or obvious behavioural signs of distress (Figure 8B). A single dose of 25 $mgkg^{-1}$ (i.p.) was toxic to animals with signs of acute toxicity observed immediately after drug administration. Using the split dose schedule (10 mgkg-1 administered i.p. once per day over 4 days), significant anti-tumour effects were observed against A2780*cis*/CP70 ($p < 0.01$), A2780 ($p = 0.01$) and OVCAR-3 ($p < 0.05$) fibres implanted intraperitoneally. Using the same schedule however, the response of fibres implanted s.c. did not reach statistical significance (Figure 8A).

4.0 Discussion:

In the search for multi-targeted anti-cancer drugs, identifying compounds that are both potent and selective towards cancer cells remains a significant challenge. A key finding of this study is that Ag8 has greater or equivalent selectivity to cisplatin *in vitro* (Figures 2, Figure S1). An enhanced level of selectivity can be obtained using non-proliferating, confluent non-cancer cells both in terms of chemosensitivity (Figure 2, Table S2) and inhibition of glycolysis (Figure 7). Moreover, that Ag8 was also well tolerated *in vivo* (Figure 8) suggests that it has a

more favourable toxicological profile than other gold-NHC complexes that have shown toxicity in *in vivo* models at comparable doses [8]. Ag8 therefore demonstrates selectivity towards cancer cells *in vitro* (particularly cisplatin resistant A2780*cis*/CP70 cells) and is well tolerated *in vivo*, especially when a split-dosing schedule is employed. Its mechanism of action is distinctly different from cisplatin (targeting multiple pathways as opposed to DNA alkylation) and this is likely to account for its ability to induce cytotoxicity in cisplatin resistant A2780 cells.

Ag8 was not tailored to a specific target and therefore a target deconvolution strategy to uncover its mechanism(s) of action was employed. The COMPARE algorithm has an established record of identifying potential mechanisms of action [24] and the chemosensitivity profile of Ag8 correlated well ($r^2 = 0.785$) with that of pleurotin, a known inhibitor of Trx-R [25]. In cell free assays, Ag8 was a very potent inhibitor of Trx-R with an IC_{50} value of 2.39 ± 0.59 nM (Figure 3). Organometallic compounds are amongst the most potent of Trx-R inhibitors and our results are consistent with these [26-29]. Mechanistically, the basis for Trx-R inhibition remains undefined but it is known that a seleno-cysteine residue at the C-terminal active site of TrxR constitutes a high affinity binding site for metal ions [30]. Trx-R is an established target for anti-cancer drug discovery [31-33] and its inhibition impacts upon multiple processes including an increase in reactive oxygen species (ROS), accumulation of the oxidised form of thioredoxin (Trx) and induction of apoptosis [34]. The results presented in Figure 3 are consistent with the inhibition of Trx-R and the induction of apoptosis via the JNK and p38 pathways [35]. It should be noted however that silver-NHC complexes have been shown to induce apoptosis via alternative pathways [36]. In contrast to other Trx-R inhibitors [25, 37], Ag8 did not alter HIF1α stability or HIF1 function (Figure S4).

The induction of ROS could contribute to the DNA damage observed in cells treated with Ag8 although an additional explanation is the ability of Ag8 to inhibit topoisomerases, particularly topoisomerase I (Figure 5). Topoisomerase enzymes are major targets for anti-cancer drugs [38, 39] and topoisomerase I inhibitors are comparatively rare. Whilst other organometallic complexes have been shown to inhibit topoisomerases [40-44], this is the first report documenting the preferential inhibition of topoisomerase I by a silver-NHC complex. The relative contribution of ROS or inhibition of topoisomerase to DNA damage induction is

not known but the induction of DNA damage by at least two different mechanisms may reduce the efficiency of DNA repair. Within the context of DNA repair, this study has demonstrated that Ag8 is a potent inhibitor of PARP-1 *in vitro* and can potentiate the activity of TMZ (Figure 6). Further studies are required to determine if the potentiation of TMZ activity is cancer selective *in vivo* and whether Ag8 can induce synthetic lethality in cells that harbour mutations in the *BRCA* genes.

Finally, metabolic reprogramming is an emerging hallmark of cancer [45] and this study has demonstrated that Ag8 can rapidly and selectively modulate aerobic glycolysis. Ag8 showed inhibitory effects on glycolysis in cancer cells but had no effect on non-proliferating ARPE-19 cells (Figure 7). Metal-based glycoconjugates including NHC carbene gold(I) complexes are of interest as glycolytic inhibitors [46, 47] but this is the first report describing a silver-NHC complex acting as a glycolytic inhibitor. The precise mechanism(s) by which Ag8 inhibits glycolysis requires further elucidation but the rapid and selective inhibition of the glycolytic phenotype in cancer in preference to non-cancer cells *in vitro* is promising.

In conclusion, the data presented herein demonstrates that Ag8 has multiple mechanisms of action involving (i) inhibition of Trx-R leading to increased ROS production and subsequently apoptosis (ii) inhibition of topoisomerase I (and to a lesser extent II) leading to DNA damage (iii) inhibition of PARP-1 leading to the potentiation of TMZ activity *in vitro* and (iv) rapid and selective inhibition of glycolysis in cancer cells. Ag8 is therefore a promising lead compound with (i) multiple mechanisms of action (ii) exhibits a degree of selectivity for cancer over normal cells that is in many instances superior to cisplatin *in vitro,* (iii) has a mechanism of action that's different from cisplatin and (iv) is well tolerated *in vivo* and has significant anti-tumour effects *in vivo* against hollow fibres implanted intraperitoneally (Figure 8). The lack of activity against fibres implanted subcutaneaously is likely to be due to the high reactivity of metal NHC complexes with biological thiols and further studies are required to address this issue [48, 49]. In a loco-regional setting however where the aim is to treat tumours that arise in a third compartment, compounds with poor systemic pharmacokinetics may paradoxically be advantageous [50].

5.0 Acknowledgements:

RMP and MS were funded by Yorkshire Cancer Research (pump priming grant BPP 046). IJS and AL were funded by NIHR Research & Innovation Division, Strategic Project Funding 2013 and Manchester Pharmacy School Fellowship. We would like to thanks Maryam Ahmadi and Zeynab Ahmedihosseini for technical assistance in conducting the work presented in figure S4.

6.0 References:

[1] F.H. Groenendijk, R. Bernards, Drug resistance to targeted therapies: deja vu all over again, Mol Oncol, 8 (2014) 1067-1083.
[2] C.E. Meacham, S.J. Morrison, Tumour heterogeneity and cancer cell plasticity, Nature, 501 (2013) 328-337.
[3] P.J. Jansson, D.S. Kalinowski, D.J. Lane, Z. Kovacevic, N.A. Seebacher, L. Fouani, S. Sahni, A.M. Merlot, D.R. Richardson, The renaissance of polypharmacology in the development of anti-cancer therapeutics: Inhibition of the "Triad of Death" in cancer by Di-2-pyridylketone thiosemicarbazones, Pharmacol Res, 100 (2015) 255-260.
[4] P. Poornima, J.D. Kumar, Q. Zhao, M. Blunder, T. Efferth, Network pharmacology of cancer: From understanding of complex interactomes to the design of multi-target specific therapeutics from nature, Pharmacol Res, 111 (2016) 290-302.
[5] A.S. Reddy, S. Zhang, Polypharmacology: drug discovery for the future, Expert Rev Clin Pharmacol, 6 (2013) 41-47.
[6] I. Romero-Canelon, P.J. Sadler, Next-generation metal anticancer complexes: multitargeting via redox modulation, Inorg Chem, 52 (2013) 12276-12291.
[7] L. Oehninger, R. Rubbiani, I. Ott, N-Heterocyclic carbene metal complexes in medicinal chemistry, Dalton Trans, 42 (2013) 3269-3284.
[8] O. Ciftci, I. Ozdemir, O. Cakir, S. Demir, The determination of oxidative damage in heart tissue of rats caused by ruthenium(II) and gold(I) N-heterocyclic carbene complexes, Toxicol Ind Health, 27 (2011) 735-741.
[9] S.J. Tan, Y.K. Yan, P.P. Lee, K.H. Lim, Copper, gold and silver compounds as potential new anti-tumor metallodrugs, Future Med Chem, 2 (2010) 1591-1608.
[10] D.C. Monteiro, R.M. Phillips, B.D. Crossley, J. Fielden, C.E. Willans, Enhanced cytotoxicity of silver complexes bearing bidentate N-heterocyclic carbene ligands, Dalton Trans, 41 (2012) 3720-3725.
[11] R.M. Phillips, P.B. Hulbert, M.C. Bibby, N.R. Sleigh, J.A. Double, In vitro activity of the novel indoloquinone EO-9 and the influence of pH on cytotoxicity, Br J Cancer, 65 (1992) 359-364.
[12] E.H. Chew, J. Lu, T.D. Bradshaw, A. Holmgren, Thioredoxin reductase inhibition by antitumor quinols: a quinol pharmacophore effect correlating to antiproliferative activity, FASEB J, 22 (2008) 2072-2083.
[13] M. Luthman, A. Holmgren, Rat liver thioredoxin and thioredoxin reductase: purification and characterization, Biochemistry, 21 (1982) 6628-6633.

[14] N.T. Georgopoulos, L.A. Kirkwood, J. Southgate, A novel bidirectional positive-feedback loop between Wnt–β-catenin and EGFR–ERK plays a role in context-specific modulation of epithelial tissue regeneration, Journal of cell science, 127 (2014) 2967-2982.
[15] S.J. Allison, J.R. Knight, C. Granchi, R. Rani, F. Minutolo, J. Milner, R.M. Phillips, Identification of LDH-A as a therapeutic target for cancer cell killing via (i) p53/NAD(H)-dependent and (ii) p53-independent pathways, Oncogenesis, 3 (2014) e102.
[16] R.T. Wheelhouse, S.A. Jennings, V.A. Phillips, D. Pletsas, P.M. Murphy, N.C. Garbett, J.B. Chaires, T.C. Jenkins, Design, synthesis, and evaluation of novel biarylpyrimidines: a new class of ligand for unusual nucleic acid structures, J Med Chem, 49 (2006) 5187-5198.
[17] W.D. Wilson, F.A. Tanious, M. Fernandez-Saiz, C.T. Rigl, Evaluation of drug-nucleic acid interactions by thermal melting curves, Methods Mol Biol, 90 (1997) 219-240.
[18] R.M. Phillips, M.A. Naylor, M. Jaffar, S.W. Doughty, S.A. Everett, A.G. Breen, G.A. Choudry, I.J. Stratford, Bioreductive activation of a series of indolequinones by human DT-diaphorase: structure-activity relationships, J Med Chem, 42 (1999) 4071-4080.
[19] R.M. Phillips, T.H. Ward, Influence of extracellular pH on the cytotoxicity and DNA damage of a series of indolequinone compounds, Anticancer Res, 21 (2001) 1795-1801.
[20] R.M. Lord, A.J. Hebden, C.M. Pask, I.R. Henderson, S.J. Allison, S.L. Shepherd, R.M. Phillips, P.C. McGowan, Hypoxia-Sensitive Metal beta-Ketoiminato Complexes Showing Induced Single-Strand DNA Breaks and Cancer Cell Death by Apoptosis, J Med Chem, 58 (2015) 4940-4953.
[21] C.L. Cheng, S.P. Johnson, S.T. Keir, J.A. Quinn, F. Ali-Osman, C. Szabo, H. Li, A.L. Salzman, M.E. Dolan, P. Modrich, D.D. Bigner, H.S. Friedman, Poly(ADP-ribose) polymerase-1 inhibition reverses temozolomide resistance in a DNA mismatch repair-deficient malignant glioma xenograft, Molecular cancer therapeutics, 4 (2005) 1364-1368.
[22] P. Workman, E.O. Aboagye, F. Balkwill, A. Balmain, G. Bruder, D.J. Chaplin, J.A. Double, J. Everitt, D.A. Farningham, M.J. Glennie, L.R. Kelland, V. Robinson, I.J. Stratford, G.M. Tozer, S. Watson, S.R. Wedge, S.A. Eccles, I. Committee of the National Cancer Research, Guidelines for the welfare and use of animals in cancer research, Br J Cancer, 102 (2010) 1555-1577.
[23] S.D. Shnyder, P.A. Cooper, A.J. Scally, M.C. Bibby, Reducing the cost of screening novel agents using the hollow fibre assay, Anticancer Res, 26 (2006) 2049-2052.
[24] S.L. Holbeck, J.M. Collins, J.H. Doroshow, Analysis of Food and Drug Administration-approved anticancer agents in the NCI60 panel of human tumor cell lines, Mol Cancer Ther, 9 (2010) 1451-1460.
[25] S.J. Welsh, R.R. Williams, A. Birmingham, D.J. Newman, D.L. Kirkpatrick, G. Powis, The thioredoxin redox inhibitors 1-methylpropyl 2-imidazolyl disulfide and pleurotin inhibit hypoxia-induced factor 1alpha and vascular endothelial growth factor formation, Mol Cancer Ther, 2 (2003) 235-243.
[26] A. Citta, E. Schuh, F. Mohr, A. Folda, M.L. Massimino, A. Bindoli, A. Casini, M.P. Rigobello, Fluorescent silver(I) and gold(I)-N-heterocyclic carbene complexes with cytotoxic properties: mechanistic insights, Metallomics, 5 (2013) 1006-1015.
[27] M. Pellei, V. Gandin, M. Marinelli, C. Marzano, M. Yousufuddin, H.V. Dias, C. Santini, Synthesis and biological activity of ester- and amide-functionalized imidazolium salts and related water-soluble coinage metal N-heterocyclic carbene complexes, Inorg Chem, 51 (2012) 9873-9882.
[28] C. Santini, M. Pellei, G. Papini, B. Morresi, R. Galassi, S. Ricci, F. Tisato, M. Porchia, M.P. Rigobello, V. Gandin, C. Marzano, In vitro antitumour activity of water soluble Cu(I), Ag(I) and Au(I) complexes supported by hydrophilic alkyl phosphine ligands, J Inorg Biochem, 105 (2011) 232-240.
[29] W. Cai, L. Zhang, Y. Song, B. Wang, B. Zhang, X. Cui, G. Hu, Y. Liu, J. Wu, J. Fang, Small molecule inhibitors of mammalian thioredoxin reductase, Free Radic Biol Med, 52 (2012) 257-265.
[30] K. Fritz-Wolf, S. Urig, K. Becker, The structure of human thioredoxin reductase 1 provides insights into C-terminal rearrangements during catalysis, J Mol Biol, 370 (2007) 116-127.

[31] J.D. Pennington, K.M. Jacobs, L. Sun, G. Bar-Sela, M. Mishra, D. Gius, Thioredoxin and thioredoxin reductase as redox-sensitive molecular targets for cancer therapy, Curr Pharm Des, 13 (2007) 3368-3377.
[32] G. Powis, D.L. Kirkpatrick, Thioredoxin signaling as a target for cancer therapy, Curr Opin Pharmacol, 7 (2007) 392-397.
[33] A. Mukherjee, S.G. Martin, The thioredoxin system: a key target in tumour and endothelial cells, Br J Radiol, 81 Spec No 1 (2008) S57-68.
[34] K.F. Tonissen, G. Di Trapani, Thioredoxin system inhibitors as mediators of apoptosis for cancer therapy, Mol Nutr Food Res, 53 (2009) 87-103.
[35] M. Saitoh, H. Nishitoh, M. Fujii, K. Takeda, K. Tobiume, Y. Sawada, M. Kawabata, K. Miyazono, H. Ichijo, Mammalian thioredoxin is a direct inhibitor of apoptosis signal-regulating kinase (ASK) 1, EMBO J, 17 (1998) 2596-2606.
[36] L. Eloy, A.S. Jarrousse, M.L. Teyssot, A. Gautier, L. Morel, C. Jolivalt, T. Cresteil, S. Roland, Anticancer activity of silver-N-heterocyclic carbene complexes: caspase-independent induction of apoptosis via mitochondrial apoptosis-inducing factor (AIF), ChemMedChem, 7 (2012) 805-814.
[37] D.T. Jones, C.W. Pugh, S. Wigfield, M.F. Stevens, A.L. Harris, Novel thioredoxin inhibitors paradoxically increase hypoxia-inducible factor-alpha expression but decrease functional transcriptional activity, DNA binding, and degradation, Clin Cancer Res, 12 (2006) 5384-5394.
[38] A.K. Larsen, A.E. Escargueil, A. Skladanowski, Catalytic topoisomerase II inhibitors in cancer therapy, Pharmacol Ther, 99 (2003) 167-181.
[39] Y. Pommier, Topoisomerase I inhibitors: camptothecins and beyond, Nat Rev Cancer, 6 (2006) 789-802.
[40] K.J. Du, J.Q. Wang, J.F. Kou, G.Y. Li, L.L. Wang, H. Chao, L.N. Ji, Synthesis, DNA-binding and topoisomerase inhibitory activity of ruthenium(II) polypyridyl complexes, Eur J Med Chem, 46 (2011) 1056-1065.
[41] R.A. Khan, A. Asim, R. Kakkar, D. Gupta, V. Bagchi, F. Arjmand, S. Tabassum, A Chloro-Bridged Heterobimetallic (eta(6)-Arene)ruthenium-Organotin Complex as an Efficient Topoisomerase I alpha Inhibitor, Organometallics, 32 (2013) 2546-2551.
[42] J.F. Kou, C. Qian, J.Q. Wang, X. Chen, L.L. Wang, H. Chao, L.N. Ji, Chiral ruthenium(II) anthraquinone complexes as dual inhibitors of topoisomerases I and II, J Biol Inorg Chem, 17 (2012) 81-96.
[43] M.N. Patel, B.S. Bhatt, P.A. Dosi, Topoisomerase inhibition, nucleolytic and electrolytic contribution on DNA binding activity exerted by biological active analogue of coordination compounds, Appl Biochem Biotechnol, 166 (2012) 1949-1968.
[44] S. Tabassum, M. Afzal, F. Arjmand, New heterobimetallic Cu(II)-Sn2(IV) complex as potential topoisomerase I inhibitor: in vitro DNA binding, cleavage and cytotoxicity against human cancer cell lines, J Photochem Photobiol B, 115 (2012) 63-72.
[45] D. Hanahan, R.A. Weinberg, Hallmarks of cancer: the next generation, Cell, 144 (2011) 646-674.
[46] R. Rubbiani, I. Kitanovic, H. Alborzinia, S. Can, A. Kitanovic, L.A. Onambele, M. Stefanopoulou, Y. Geldmacher, W.S. Sheldrick, G. Wolber, A. Prokop, S. Wolfl, I. Ott, Benzimidazol-2-ylidene gold(I) complexes are thioredoxin reductase inhibitors with multiple antitumor properties, J Med Chem, 53 (2010) 8608-8618.
[47] G.L. Robinson, D. Dinsdale, M. Macfarlane, K. Cain, Switching from aerobic glycolysis to oxidative phosphorylation modulates the sensitivity of mantle cell lymphoma cells to TRAIL, Oncogene, 31 (2012) 4996-5006.
[48] T.T. Fong, C.N. Lok, C.Y. Chung, Y.M. Fung, P.K. Chow, P.K. Wan, C.M. Che, Cyclometalated Palladium(II) N-Heterocyclic Carbene Complexes: Anticancer Agents for Potent In Vitro Cytotoxicity and In Vivo Tumor Growth Suppression, Angew Chem Int Ed Engl, 55 (2016) 11935-11939.
[49] T. Zou, C.T. Lum, C.N. Lok, W.P. To, K.H. Low, C.M. Che, A binuclear gold(I) complex with mixed bridging diphosphine and bis(N-heterocyclic carbene) ligands shows favorable thiol reactivity and inhibits tumor growth and angiogenesis in vivo, Angew Chem Int Ed Engl, 53 (2014) 5810-5814.

[50] R.M. Phillips, H.R. Hendriks, G.J. Peters, E. Pharmacology, G. Molecular Mechanism, EO9 (Apaziquone): from the clinic to the laboratory and back again, Br J Pharmacol, 168 (2013) 11-18.

Figure legends:

Figure 1. Chemical Structure of Ag8. The synthesis and chemical characterisation is described elsewhere [10].

Figure 2. Response of cancer and non-cancer cell lines to Ag8 and cisplatin. (A) The response of a panel of cancer cells following continuous exposure to cisplatin or Ag8. Data are mean ± standard deviation for 3 independent experiments. (B) The selectivity index was determined as the IC_{50} for sub-confluent (sc) or confluent (c) non-cancer cells (ARPE-19, WI38 or PNT2) divided by the IC_{50} for either A2780 or A2780cis/CP70 cells. Confluent non-cancer cells were included to reflect the fact that the majority of normal cells are non-proliferating. Cisplatin was tested against confluent PNT2 cells only. The legend embedded in the figure is common to all three data sets. Values > 1 denote preferential activity against cancer compared to non-cancer cells whereas values ≤ 1 denote equitoxic or reduced activity against cancer cells compared to non-cancer cells.

Figure 3. Induction of oxidative stress by Ag8. (A) Dose dependent inhibition of purified rat thioredoxin reductase by Ag8. Data are mean ± standard deviation for ≥ 3 independent experiments. (B) Induction of ROS in A2780 cells following exposure (1 h) to Ag8 (10μM) or cisplatin (10μM) as determined by H2-DCFDA labelling and flow cytometry. The panel is an overlay histogram of representative fluorescence measurements (from 3 independent experiments). MFI, Mean Fluorescent Intensity. (C) The effect of the anti-oxidant NAC on the activity of Ag8 and cisplatin against A2780 and A2780*cis*/CP70 cells is presented in

panel C. The bars show mean % survival values ± SD (n = 3) at the doses specified. (D) Following treatment of the A2780*cis*/CP70 and A2780 cell lines with Cisplatin and Ag8 (10μM) at the indicated time points, the relative levels of phospho-p38 (Thr180/Tyr182) and phospho-JNK (Thr183/Try185) were determined by immunoblotting. Equal loading was determined by assessing the levels of β-actin.

Figure 4: Induction of apoptosis by Ag8. Induction of apoptosis (open bars) or late apoptosis/necrosis (shaded bars) was measured in A2780 (A) and A2780*cis*/CP70 (B) cells following exposure to etoposide, cisplatin and Ag8. Cells were exposed to drug (10 μM, 24 h) and apoptosis and late apoptosis/necrosis were determined by FACS analysis using annexin-V and propidium iodide staining respectively. Results show the mean percentage of cells ± SD (n = 3).

Figure 5. DNA Interaction and damage induction in cell-free and cell-based assays. (A) Thermal melting profiles of calf thymus DNA in the absence and presence of Ag8 (from l to r, [Ag8] = 0, 1, 2, 3, 5, 7 μM). Variation in ΔT_m and ΔT_m^{80} and ΔT_m^{20} with ligand:bp ratio is presented in Figure S5. (B) the induction of DNA strand breaks by measuring the conversion of supercoiled (SC) to open circular (OC) plasmid DNA in the presence of increasing doses of EO9 (positive control) and Ag8. For EO9, lane 1 is control, lanes 2 to 10 contain 2-fold incremental increases in EO9 concentration (from 39 nM in lane 2 to 10 μM in lane 10); lane 11 contains EO9 (10 μM) in the presence of the NQO1 inhibitor dicoumarol (2 mM). For Ag8, lane 1 is control, lanes 2 to 11 contain 2-fold incremental increases in Ag8 (from 200 nM in lane 2 to 100 μM in lane 11. (C, D, E) Results of comet assays in A2780 (open bars) and A2780 CP70 (solid bars) cells. The inset images show comets for control (C) and treated (T) cells. The induction of single strand breaks (SSB, panel C), SSB and double strand breaks (DSB, panel D) and DNA cross-links (panel E) at various doses of Ag8 were quantified using Comet Assay III software. Panels A and C are results of the alkaline comet assay whereas panel B is the results of the neutral comet assay. Each value represents the mean ± SD (n=3). (F) the ability of Ag8 to inhibit human topoisomerase I and II in a cell free assay. Controls 1 and 2 represent assays run without and with either topoisomerases I or II respectively. No Ag8 was included in these controls and the final DMSO concentration was 0.1% (v/v) in all samples. R and SC denote relaxed and supercoiled forms of the plasmid respectively.

Figure 6. Inhibition of PARP activity by Ag8. (A) Dose-dependent inhibition of recombinant PARP1 activity by Ag8 as determined by levels of histone PARylation in a cell-

free ELISA. Inhibition of recombinant PARP1 by PARP inhibitor NU1025 is shown for comparison. PARP activity is expressed as a % relative to recombinant PARP1 activity in the absence of Ag8 or NU1025, mean ± SD (n=3). (B) Scheme outlining the experimental design used to assay whether Ag8 can affect PARP DNA repair activity in cultured cells. (C-F) Cells were seeded on coverslips and after 24h exposed to TMZ (1mM, 2 h) to induce single-strand DNA breaks (SSBs). TMZ was then removed and cells washed and incubated in fresh cell culture medium in the presence or absence of Ag8 or NU1025 for a further 15h to allow time for DNA repair of SSBs. Inhibition of PARP prevents SSB repair resulting in collapsed replication forks and the generation of double strand breaks (DSBs). DSBs were specifically detected via cell staining for γH2AX phosphorylation at S139. Representative immunofluorescent images of cells after 15h 'repair' time in fresh medium ± Ag8 or PARP inhibitor NU1025. Left hand panels, DAPI staining to visualise cell nuclei; centre panels, cells immunostained for phosphorylated S139 γH2AX (marker of DSBs); right hand panels, merged images showing both DAPI and S139P γH2AX staining. (G) The potentiation of TMZ activity by Ag8 or the PARP inhibitor NU1025. Cells were treated with TMZ (500μM) or solvent control and incubated in the presence or absence of the indicated concentrations of Ag8 or NU1025 (100μM) for 4 days. Effects on cell survival were determined by the MTT assay.

Figure 7. Ag8 selectively inhibits glycolysis and reduces glycolytic capacity in tumour cells. Effects on glycolytic parameters in A2780 and OVCAR3 tumour cells and the non-cancer cell line ARPE-19 following exposure to Ag8 (1 μM, given to cells immediately prior to (acute), 30 min or 60 min before the Seahorse assay). The assay measures changes in extracellular pH as an indicator of glycolytic activity. Basal extracellular acidification is measured during a 20 min equilibration in glucose free media, then glucose is the added to induce glycolysis, and changes in pH are measured for a further 25 minutes. Glycolysis is assessed as the difference in pH prior to and after the addition of glucose. The next step in the assay is to add oligomycin, which forces cells to utilize glucose as their energy source. Measurements of pH are then made for a further 25 minutes. Glycolytic capacity is assessed as the difference in pH seen following oligomycin treatment compared to the basal measurement (Panel B). All results are the mean ± SEM for at least three independent experiments and all three exposure times to Ag8 were carried out on the same day using the same passage number of cells. Statistical comparisons were performed using students t-test and *, $^{+}$ and $^{\$}$ represent p values of <0.05, <0.005 and <0.0001 respectively.

Figure 8. Activity of Ag8 against a panel of ovarian cancer cells *in vivo* in the hollow fibre assay. Each cell line was implanted either intraperitoneally (i.p.) or subcutaneously (s.c.) in mice and treated with Ag8 (10 $mgkg^{-1}$) administered i.p. on days 3,4,5 and 6 after implantation. The open and solid bars (panel A) represent control and treated fibres and values are mean ± SD for ≥6 hollow fibres. Statistical analysis was conducted using the Students t-test and ** and * indicate significance at $p < 0.01$ and $p < 0.05$ respectively. The results of dose escalation studies and toxicity assessments are presented in panel B. Toxicity was defined as (i) >10% loss in body weight measured over a two week period and (ii) assessment of acute toxicity in the form of behavioral signs of stress in animals over a 24 hour period following drug administration.

Figure 1

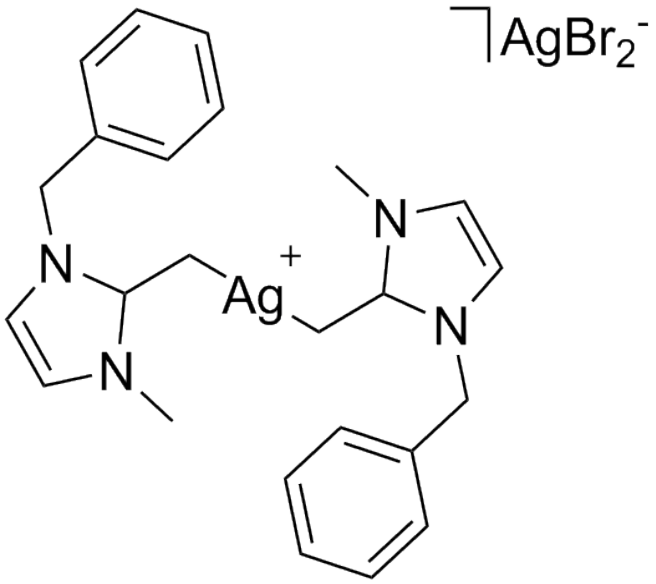

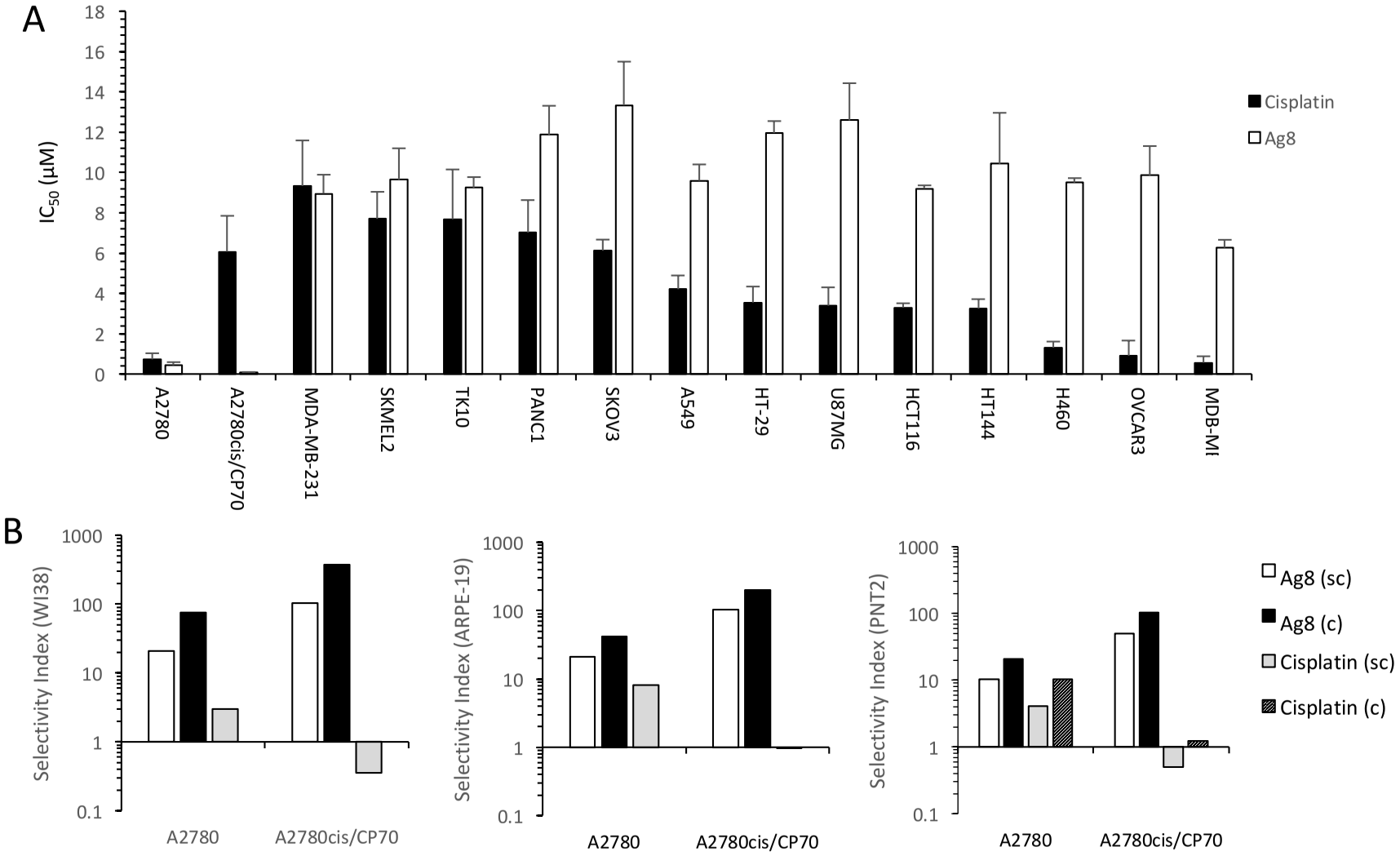
A
IC50 (μM)
18
16
14
12
10
8
6
4
2
0
Cisplatin
Ag8
A2780
A2780cis/CP70
MDA-MB-231
SKMEL2
TK10
PANC1
SKOV3
A549
HT-29
U87MG
HCT116
HT144
H460
OVCAR3
MDB-MI
B
Selectivity Index (WI38)
Selectivity Index (ARPE-19)
Selectivity Index (PNT2)
1000
100
10
1
0.1
A2780
A2780cis/CP70
Ag8 (sc)
Ag8 (c)
Cisplatin (sc)
Cisplatin (c)

Figure 2

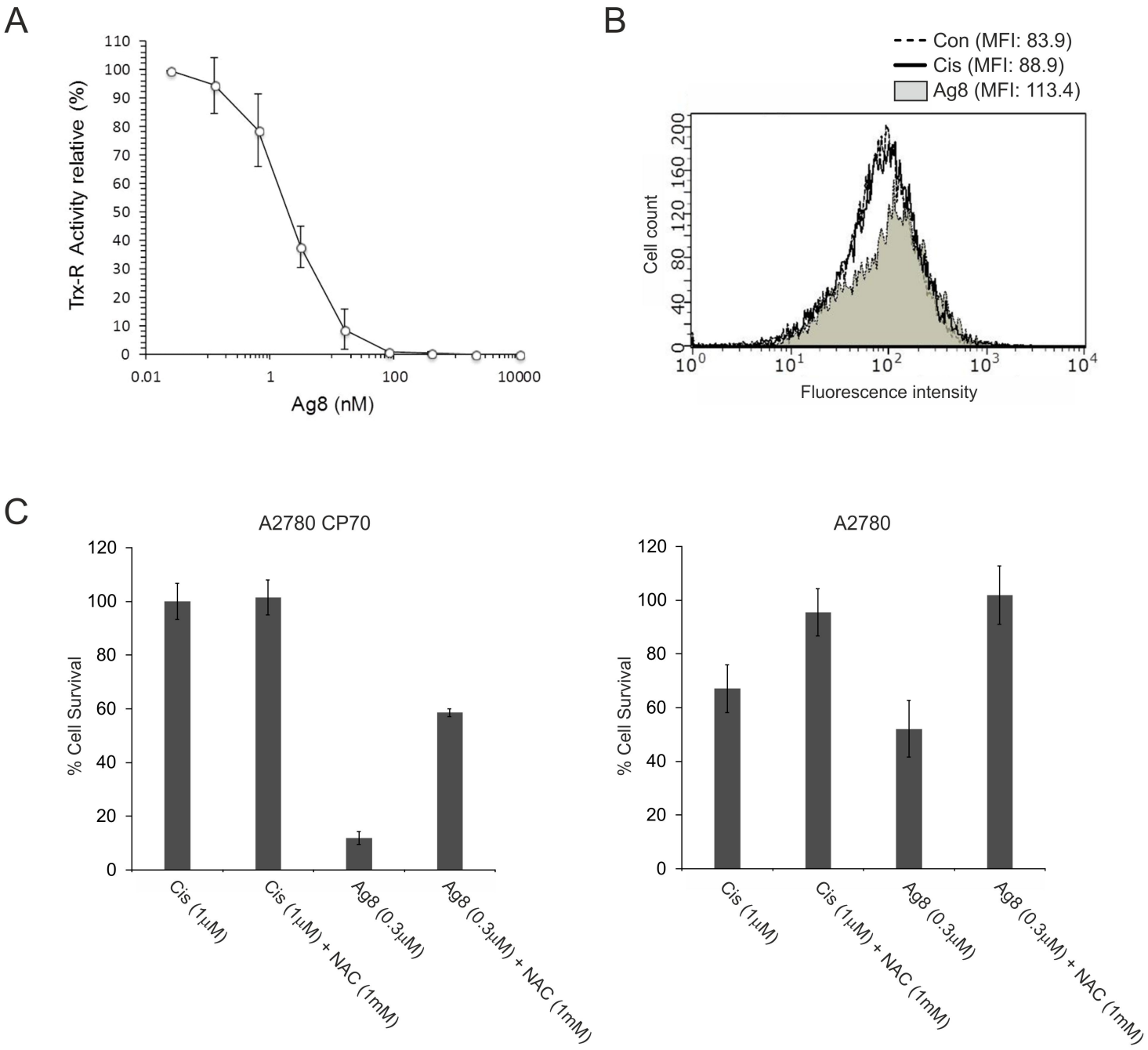
A
Trx-R Activity relative (%)
Ag8 (nM)
B
Con (MFI: 83.9)
Cis (MFI: 88.9)
Ag8 (MFI: 113.4)
Cell count
Fluorescence intensity
C
A2780 CP70
A2780
% Cell Survival
Cis (1μM)
Cis (1μM) + NAC (1mM)
Ag8 (0.3μM)
Ag8 (0.3μM) + NAC (1mM)
D
A2780 CP70
A2780
10μM Cis
10μM Ag8
Time (h)
Mw (kDa)
p-p38
β-actin
p-JNK
38
42
54 (JNK2)
46 (JNK1)

Figure 4

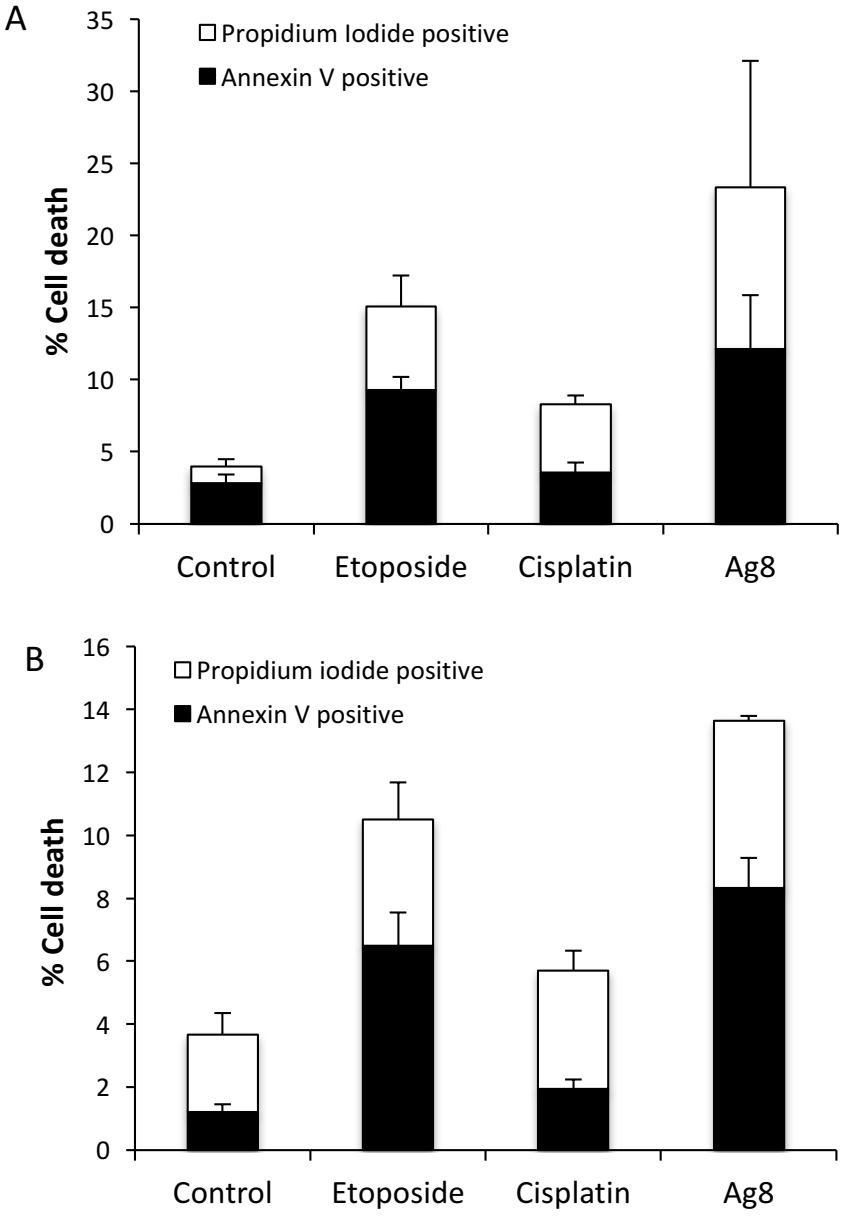
A
Propidium Iodide positive
Annexin V positive
% Cell death
35
30
25
20
15
10
5
0
Control
Etoposide
Cisplatin
Ag8
B
Propidium iodide positive
Annexin V positive
% Cell death
16
14
12
10
8
6
4
2
0
Control
Etoposide
Cisplatin
Ag8

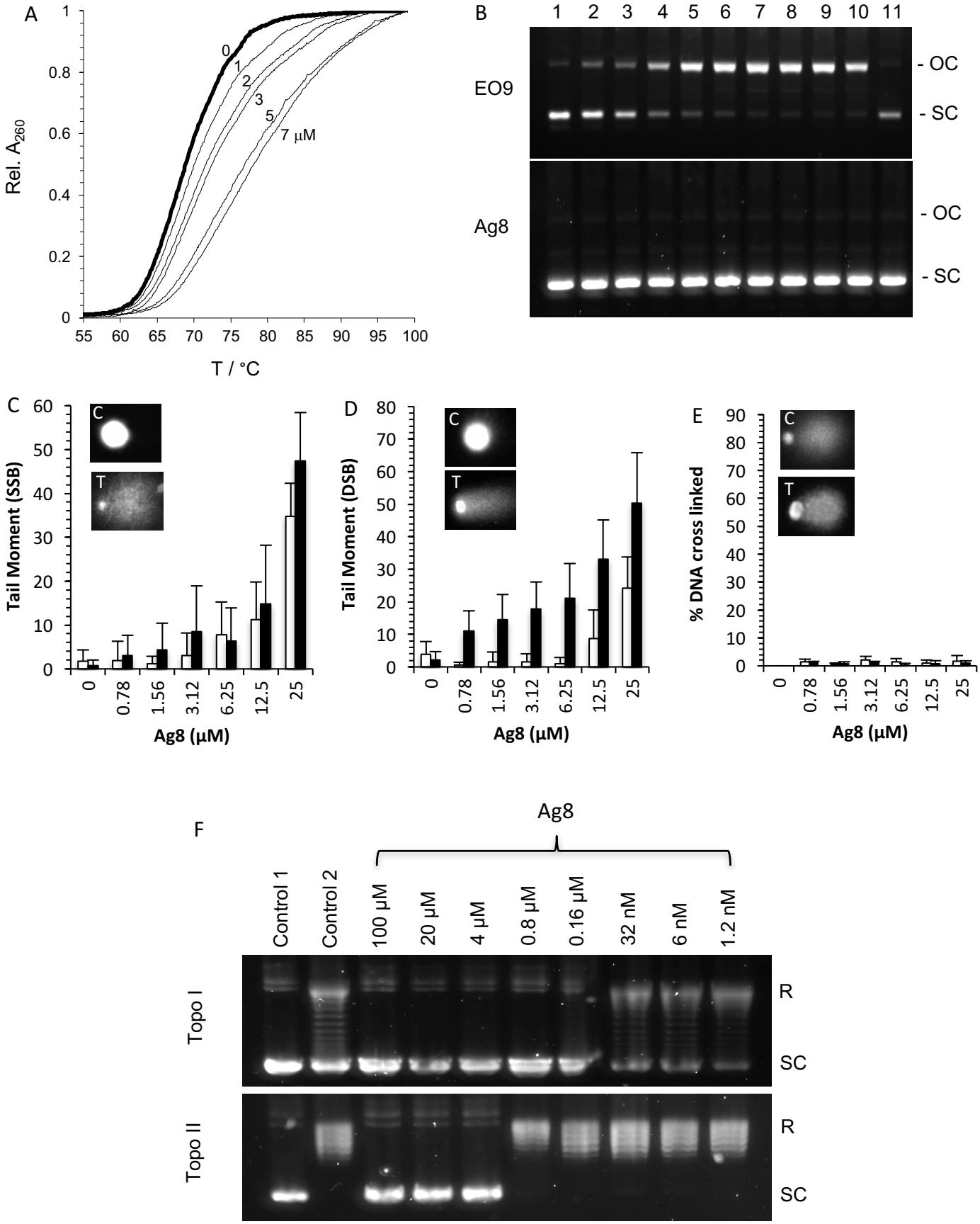
A
Rel. A_{260}
T / °C
0
1
2
3
5
7 μM
B
1 2 3 4 5 6 7 8 9 10 11
EO9
Ag8
- OC
- SC
C
Tail Moment (SSB)
Ag8 (μM)
D
Tail Moment (DSB)
Ag8 (μM)
E
% DNA cross linked
Ag8 (μM)
F
Ag8
Control 1
Control 2
100 μM
20 μM
4 μM
0.8 μM
0.16 μM
32 nM
6 nM
1.2 nM
Topo I
Topo II
R
SC

Figure 5

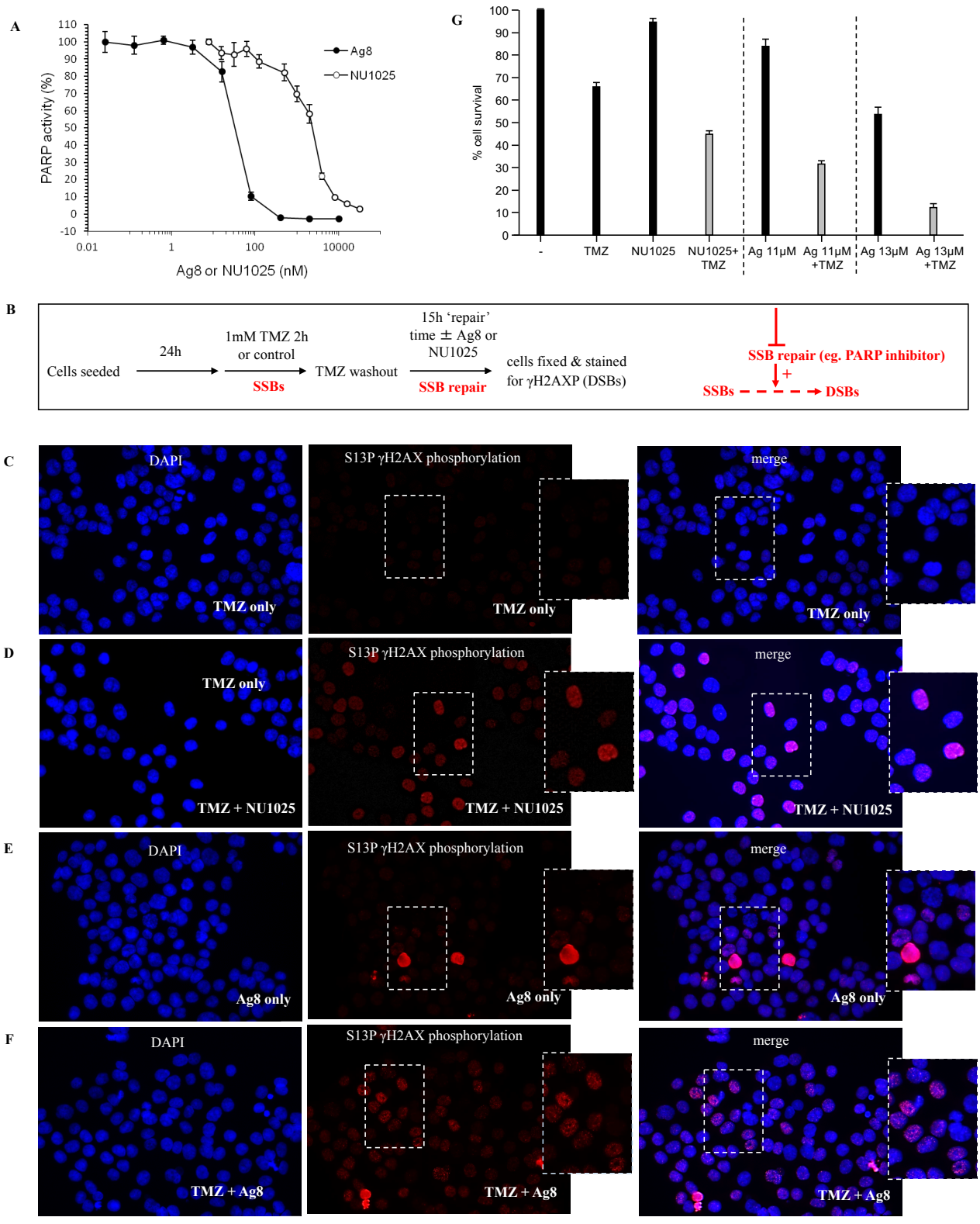
A
PARP activity (%)
Ag8
NU1025
Ag8 or NU1025 (nM)
G
% cell survival
-
TMZ
NU1025
NU1025+ TMZ
Ag 11μM
Ag 11μM +TMZ
Ag 13μM
Ag 13μM +TMZ
B
Cells seeded
24h
1mM TMZ 2h or control
SSBs
TMZ washout
15h 'repair' time ± Ag8 or NU1025
SSB repair
cells fixed & stained for γH2AXP (DSBs)
SSB repair (eg. PARP inhibitor)
+
SSBs
DSBs
C
DAPI
TMZ only
S13P γH2AX phosphorylation
TMZ only
merge
TMZ only
D
TMZ only
TMZ + NU1025
S13P γH2AX phosphorylation
TMZ + NU1025
merge
TMZ + NU1025
E
DAPI
Ag8 only
S13P γH2AX phosphorylation
Ag8 only
merge
Ag8 only
F
DAPI
TMZ + Ag8
S13P γH2AX phosphorylation
TMZ + Ag8
merge
TMZ + Ag8

Figure 7

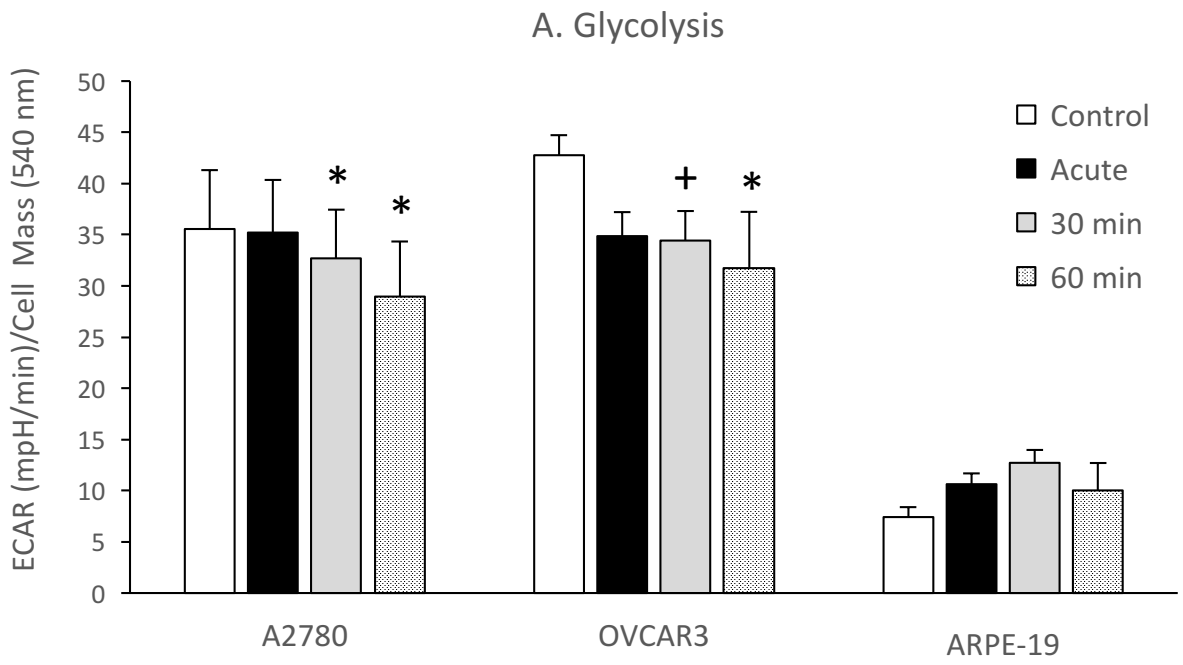
A. Glycolysis
ECAR (mpH/min)/Cell Mass (540 nm)
50
45
40
35
30
25
20
15
10
5
0
*
*
+
*
Control
Acute
30 min
60 min
A2780
OVCAR3
ARPE-19

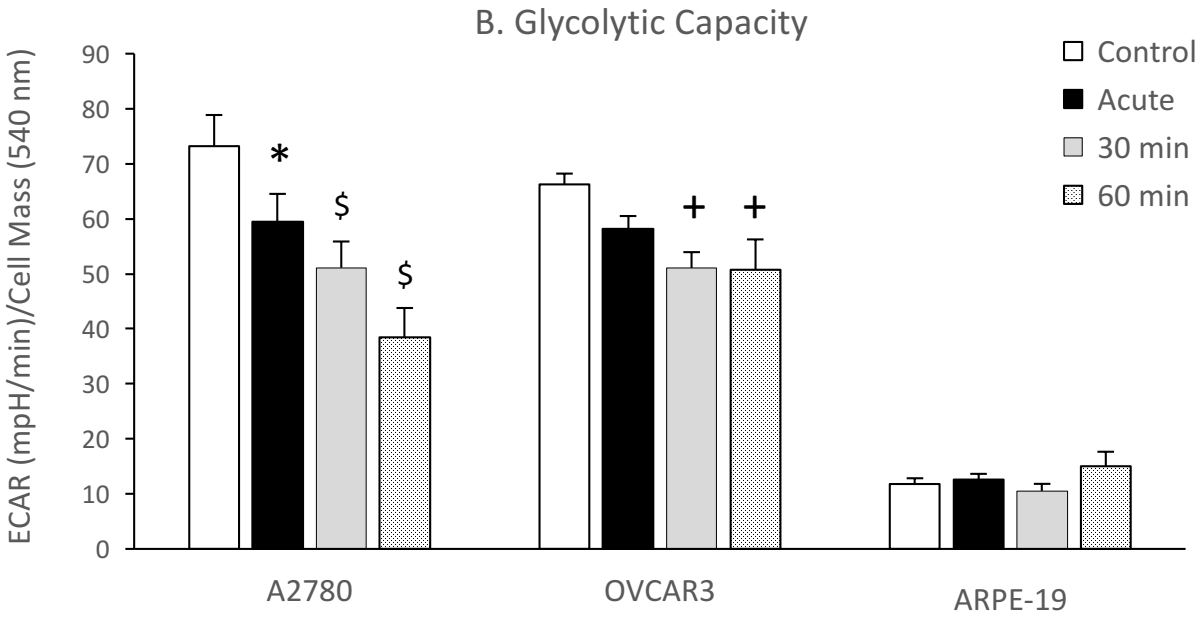
B. Glycolytic Capacity
ECAR (mpH/min)/Cell Mass (540 nm)
90
80
70
60
50
40
30
20
10
0
*
$
$
+
+
Control
Acute
30 min
60 min
A2780
OVCAR3
ARPE-19

Figure 8

A

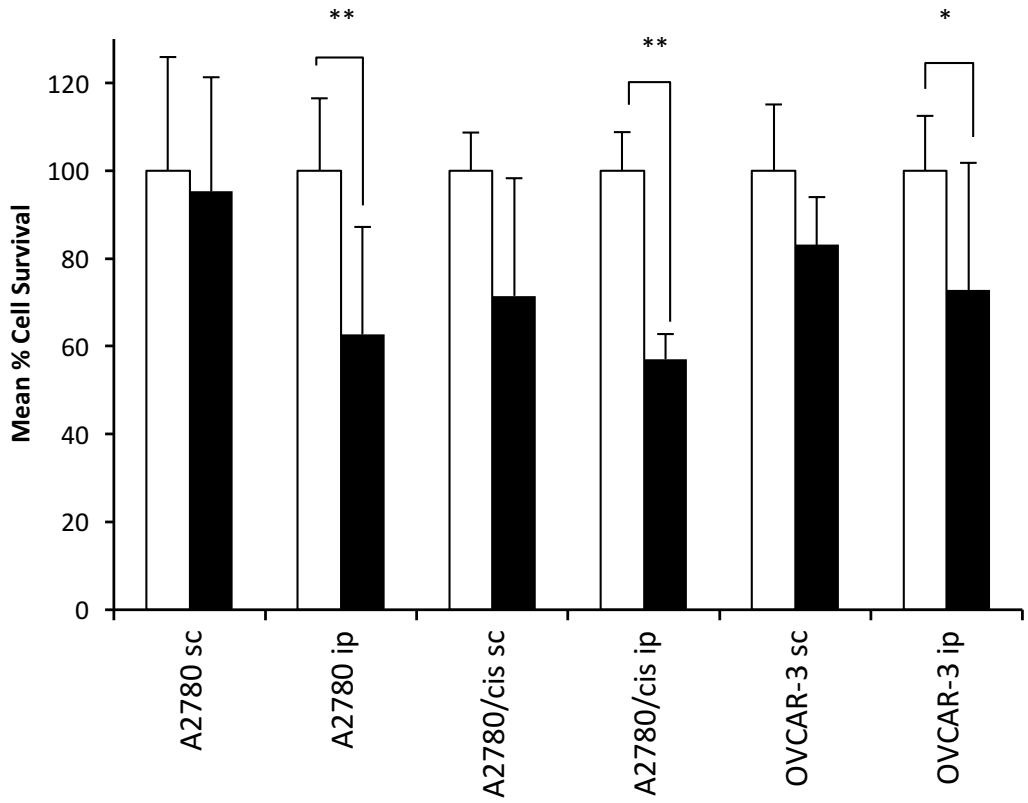

B

Dose (mg/kg)	Administration	Route	Outcome
10	Single bolus	i.p.	Not toxic
20	Single bolus	i.p.	Not toxic
25	Single bolus	i.p.	Toxic
4	Single dose given once a day for 4 days	i.p.	Not toxic
10	Single dose given once a day for 4 days	i.p.	Not toxic

Supplementary data information:

Figure S1

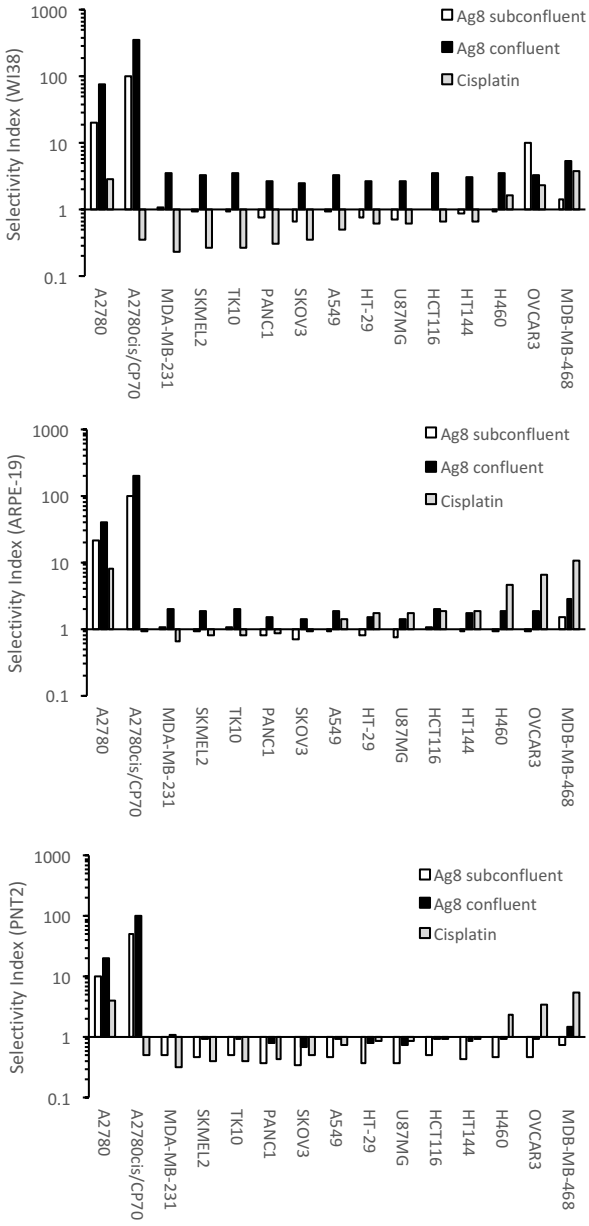

Figure S1. Response of a panel of cancer cell lines relative to the non-cancer cell lines ARPE-19, WI38 and PNT2. The results are expressed as Selectivity Indices defined as the IC_{50} of non-cancer cells divided by the IC_{50} of cancer cells. Values >1 indicate selective activity against cancer cells. For Ag8, selectivity indices were calculated using the IC_{50} values for sub-confluent, proliferating and confluent, non-proliferating non-cancer cells.

Figure S2

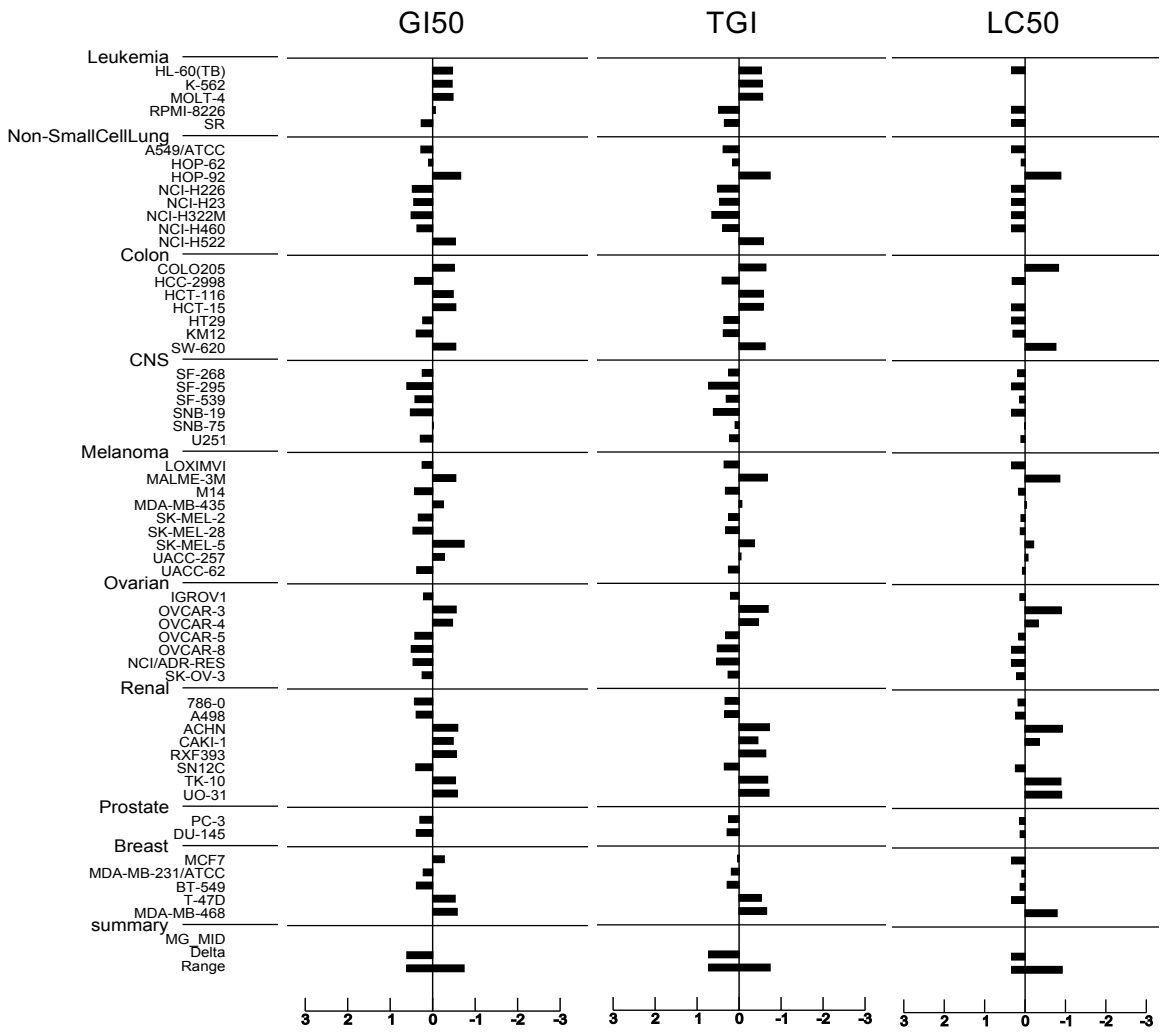

Figure S2: Chemosensitivity fingerprints for Ag8. Ag8 was submitted for evaluation in the NCI60 panel of human tumour cells (NSC767019).

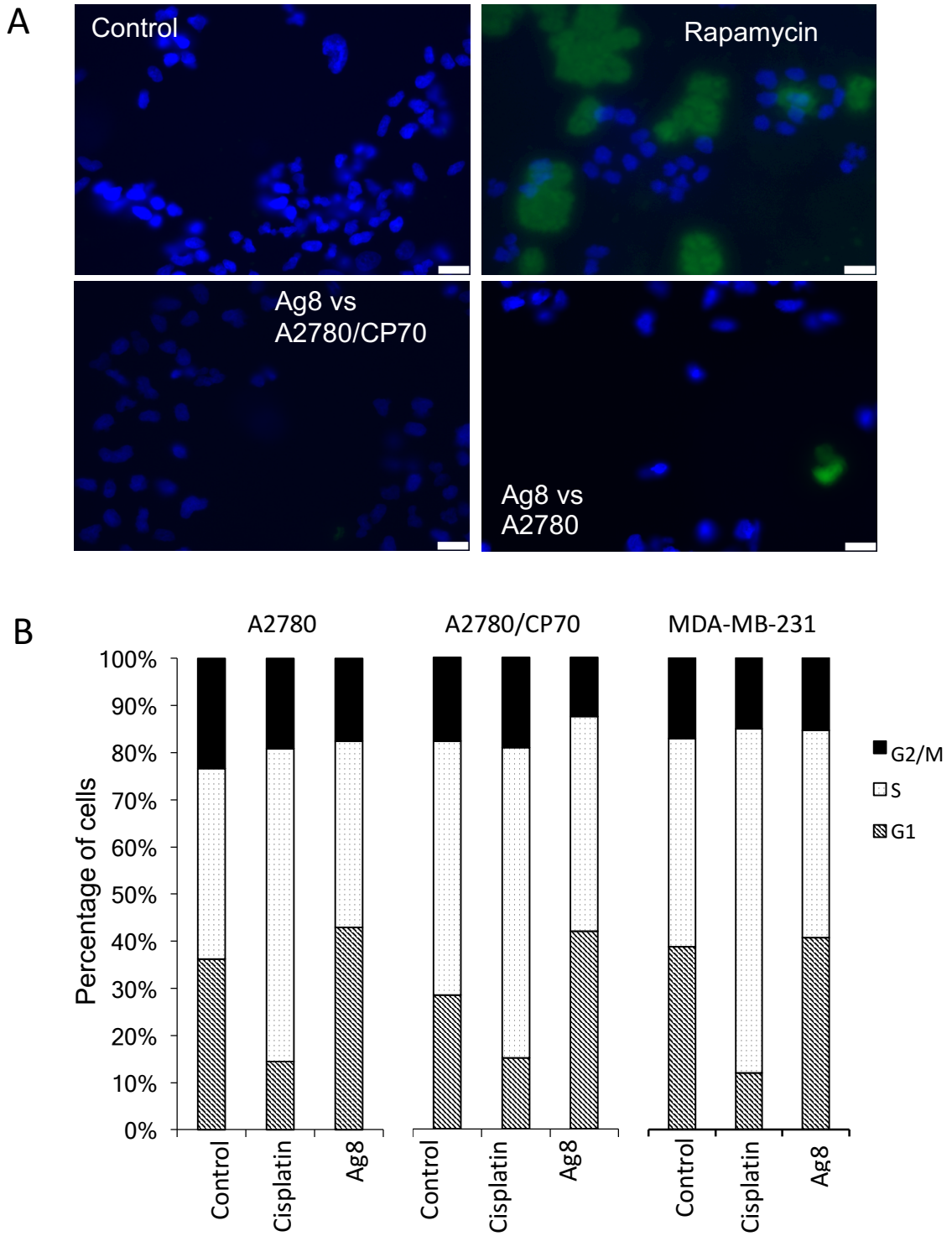

Figure S3: Induction of autophagy by Ag8 and the effect of Ag8 on cell cycle kinetics. (A) Induction of autophagy in A2780 and A2780*cis*/CP70 cells was determined using the Cyto-ID® Autophagy Detection Kit (Enzo Life Sciences). Cells at a density of 1×10^5 cells/ml were grown on glass coverslips in medium (2 ml) and incubated overnight at 37 °C, 5%CO_2. Cells were exposed to Ag8 (10 μM) or the positive control, rapamycin (500 nM) for 24 h at 37 °C, after which the protocol was followed as described in the manufacturer's guide. Whilst rapamycin induced autophagy, Ag8 did not induce autophagy. (B) The effect of Ag8 and cisplatin on cell cycle kinetics determined using the GenScript Cell Cycle Analysis Kit. In brief, A2780, A2780*cis*/CP70 and MDA-MB-231 were seeded at a density of 5×10^4 cells/ml in 6-well plates and incubated overnight at 37 °C, 5% CO_2. Cells were treated with Ag8 or cisplatin (10 μM, 24 h) following which, cells were harvested by trypsinisation and stained with propidium iodide as per manufacturer's instructions.

Figure S4

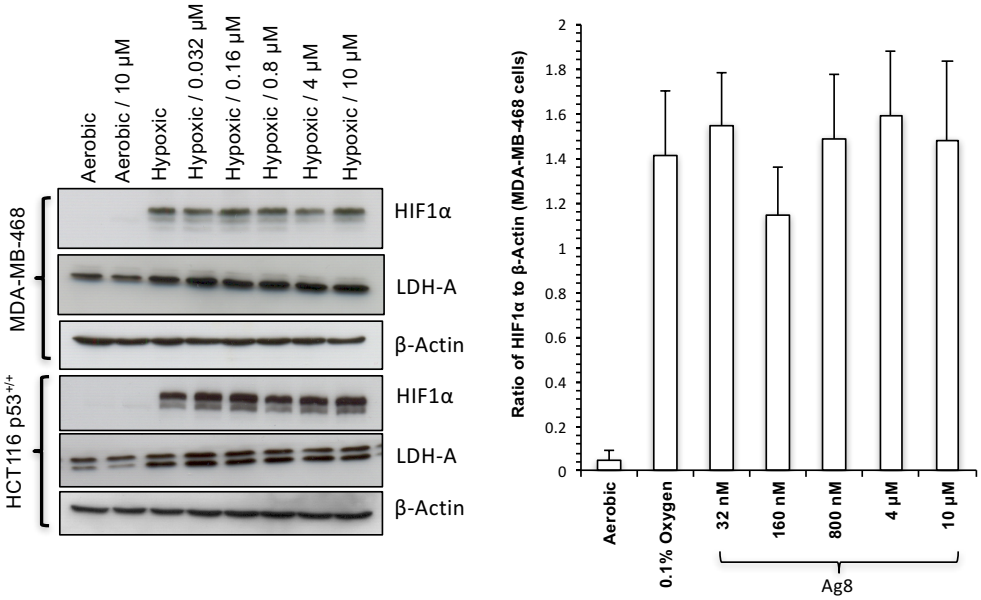

Figure S4: Influence of Ag8 on HIF1α expression and HIF1 activity. MDA-MB-468 and HCT116p53$^{+/+}$ cells were initially pre-treated with Ag8 (at the doses indicated in the figure) under aerobic conditions for 1 h. Treated cells were then transferred to hypoxic conditions (0.1% oxygen) without changing the media and incubated for a further 24 hours prior to lysing for Western blot analysis. Under aerobic conditions, Ag8 at 10µM did not induce HIF1α or lactate dehydrogenase A (LDH-A). Exposure of both HCT116p53$^{+/+}$ and MDA-MB-468 cells to hypoxia alone led to a significant induction of HIF1α protein and LDH-A. Ag8 at a range of concentrations did not alter the expression of both HIF1α or LDH-A under hypoxic conditions.

Figure S5

A

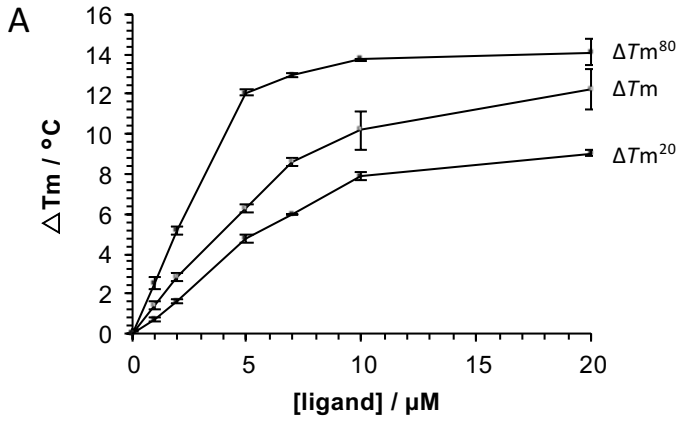

B

Ag8 (µM)	ΔT_m / °C[a]	ΔT_m^{80} / ΔT_m^{20}[c]
1	1.4	3.5
2	2.9	3.2
5	6.3	2.5
7	8.6	2.2
10	10.2[b]	1.7[d]
20	12.3[b]	1.6[d]

Figure S5. Analysis of thermal melting profiles of ctDNA in the presence and absence of Ag8. (A) ΔT_m, ΔT_m^{80} and ΔT_m^{20} values are taken from the scaled data (Figure 5 A) error bars are the range (n=2) or SD (n=3) of two or three determinations. All solutions contained 0.1% DMSO. (B) ΔT_m values in the presence of Ag8. [a]ΔT_m = T_m(DNA+ligand) – T_m(DNA). T_m for ctDNA = 68.8 °C, ΔT_m is the point of inflection in the thermal melting curve; [b]dissociation was incomplete at 99 °C so ΔT_m vales are graphical estimates for which errors are estimated as ±1 °C; [c]ΔT_m^{80} and ΔT_m^{20} values were taken from the scaled data, errors are the range (n=2) or SD (n=3) of two or three determinations; [d]interpolated values. Data show preferential stabilisation of GC-rich sequences at lower Ag8 concentrations (ΔT_m^{80} / ΔT_m^{20} >>1) and then stabilization of AT-sequences at higher Ag8 concentrations (ΔT_m^{80} / ΔT_m^{20} tends towards 1).

Figure S6

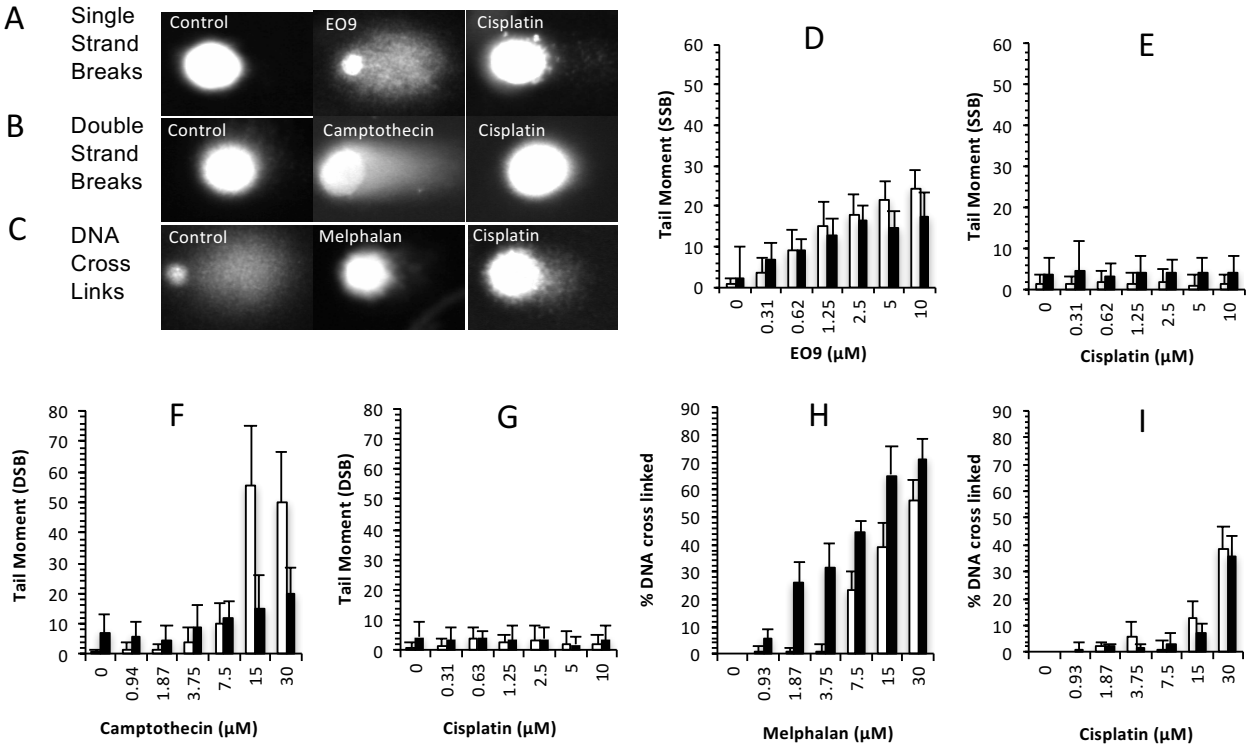

Figure S6: Comet assay analysis of DNA damage induction in A2780 and A2780*cis*/CP70 cell lines *in vitro* by positive control compounds. Single strand breaks (SSB) and cross link analysis were performed using the alkaline comet assay whereas combined SSB and double strand breaks (DSB) was determined using the neutral comet assay. (A-C) Representative images of comets obtained in the A2780 cell line for single strand breaks (SSB), double strand breaks (DSB) and cross links. (D-I) EO9, camptothecin and melphalan were used as positive controls for SSB, DSB and DNA cross link formation respectively. All compounds were obtained from Sigma Aldrich with the exception of EO9 which was a gift from Spectrum Pharmaceuticals (USA). Quantitation of dose dependent induction of DNA damage in A2780 (open bars) and A2780/CP70 (solid bars) is presented in panel D. Each value represents the mean ± SD (n=3).

Figure S7

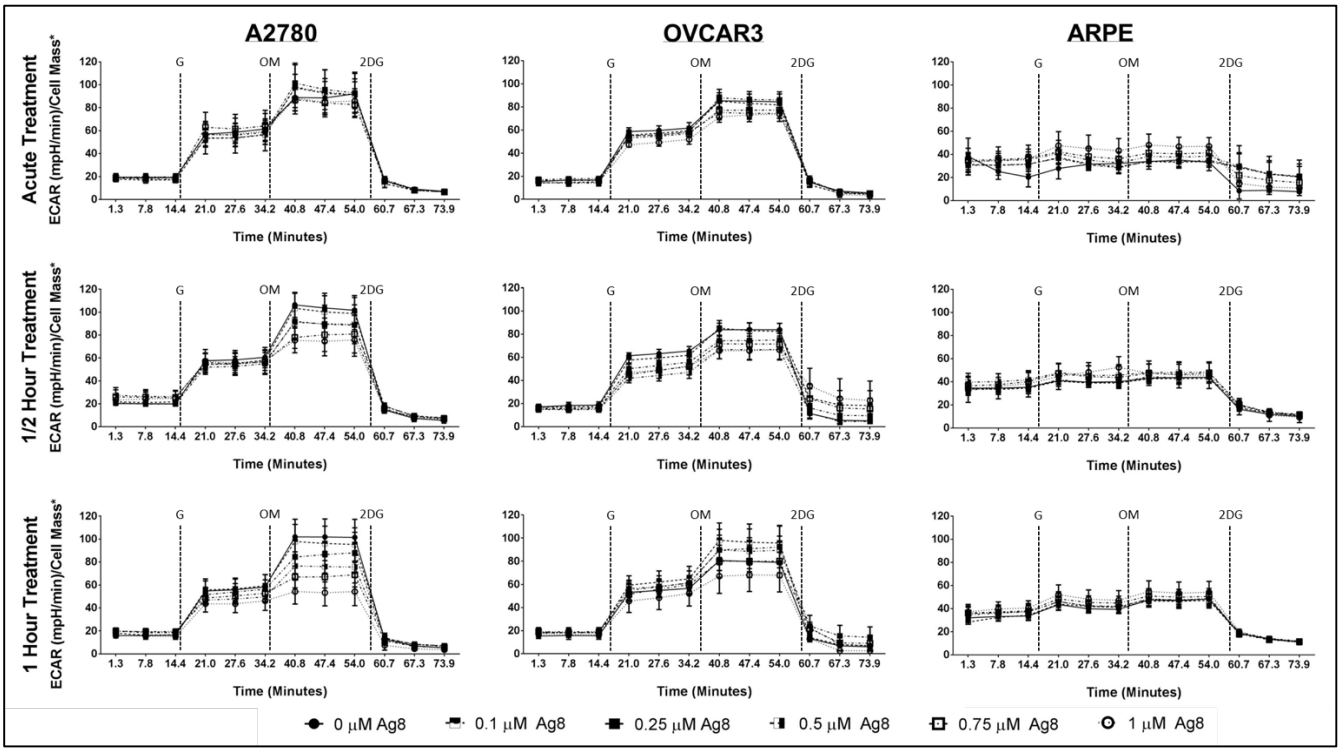

Figure S7: Glycolysis stress test profiles for all cell lines tested. The results shown for three different time points tested: acute (upper panels), 30 min (middle panels) and 1 h (lower panels) treatment with Ag8 over a range of concentrations. Dashed line indicates injection time for G: Glucose, OM: Oligomycin and 2DG: 2-deoxyglucose. *Cell mass determined as absorbance at 550 nm.

Figure S8:

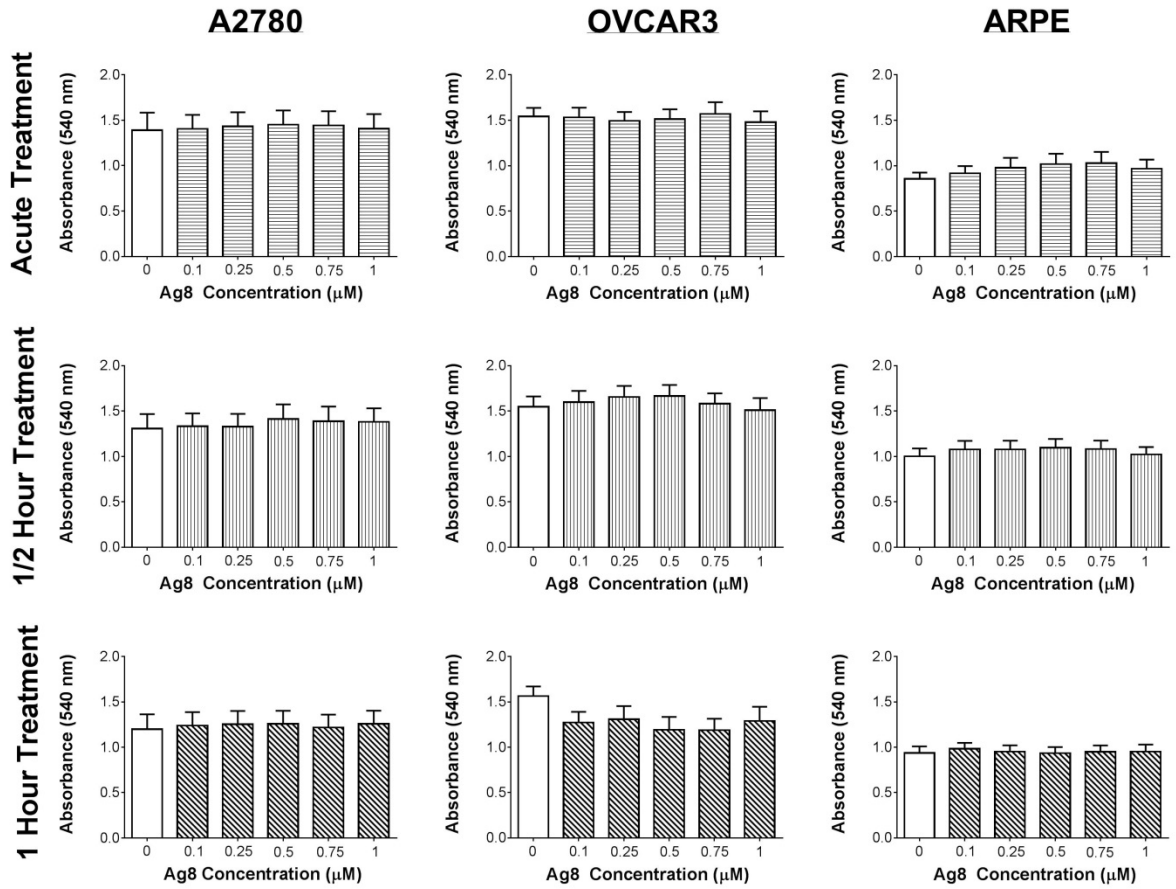

Figure S8: SRB results for 3 different cell lines (A2780, OCVAR3 and ARPE-19) treated with different concentrations of Ag8 (0-1 μM) at 3 different time points. The upper, middle and lower panels show acute, 30 min and 60 min exposure to Ag8 respectively. Open bars represent non-drug treated controls in all cases. The results demonstrate that Ag8 under these experimental conditions is not causing a reduction in cellular biomass.

Table S1

Cell line	Histological Origin	Source
A2780	Ovarian Carcinoma	ECACC
A2780 *cis*/CP70	Ovarian Carcinoma	ECACC
SKOV3	Ovarian Carcinoma	ATCC
OVCAR-3	Ovarian Carcinoma	ATCC
MDA-MB-231	Breast Adenocarcinoma	ATCC
MDA-MB-468	Breast Adenocarcinoma	ATCC
A549	Non- Small Cell Lung Carcinoma	ATCC
H460	Non- Small Cell Lung Carcinoma	ATCC
HT-29	Colorectal Adenocarcinoma	ATCC
HCT116 $p53^{+/+}$	Colorectal Carcinoma	
SK-MEL-2	Malignant Melanoma	ATCC
HT-144	Malignant Melanoma	ATCC
U87-MG	Glioblastoma	ATCC
PANC-1	Pancreatic epithelioid carcinoma	ATCC
ARPE-19	Retinal Pigmented Epithelium	ATCC
WI-38	Lung fibroblast	ATCC
PNT2	Prostate Epithelium	ECACC

Table S1. List of cell lines used, their histological origin and source of cells. ECACC denotes European Collection of Authenticated Cell Lines and ATCC denotes American Type Culture Collection.

Table S2

Cell line	Ag8 IC_{50} (μM)	Cisplatin IC_{50} (μM)
ARPE-19 (sc)	9.3 ± 0.06	5.97 ± 0.95
ARPE-19 (c)	18.17 ± 0.24	-
WI38 (sc)	9.2 ± 0.16	2.17 ± 0.74
WI38 (c)	33.32 ± 0.88	-
PNT2 (sc)	4.52 ± 0.26	3.02 ± 0.43
PNT2 (c)	9.18 ± 0.52	7.54 ± 0.37

Table S2: Response of non-cancer cell lines to Ag8 and cisplatin. Cells were exposed to Ag8 or Cisplatin for 96 h before cell survival was determined using the MTT assay. Compounds were tested against sub-confluent (sc) or confluent (c) cells and each IC_{50} value represents the mean ± standard deviation for three independent experiments.